

The Voronoi Diagram of Four Lines in \mathbb{R}^3

Evanthia Papadopoulou ✉ 

Faculty of Informatics, Università della Svizzera italiana (USI), Lugano, Switzerland

Zeyu Wang ✉ 

Faculty of Informatics, Università della Svizzera italiana (USI), Lugano, Switzerland

Abstract

We consider the Voronoi diagram of lines in \mathbb{R}^3 under the Euclidean metric, and give a full classification of its structure in the base case of four lines in general position. We first show that the number of vertices in the Voronoi diagram of four lines in general position is always even, between 0 and 8, and all such numbers can be realized. We identify a key structure for the diagram formation, called a *twist*, which is a pair of consecutive intersections among trisector branches; only two types of twists are possible, so-called *full* and *partial* twists. A full twist is a purely local structure, which can be inserted or removed without affecting the rest of the diagram. Assuming no full twists, the nearest and the farthest Voronoi diagrams of four lines, each have 15 distinct topologies, which are in one-to-one correspondence; the two-dimensional faces are all unbounded, and the total number of vertices is at most six. The unbounded features of the farthest diagram, encoded in a two-dimensional spherical map, are also in one-to-one correspondence. The identified topologies are all realizable. Any Voronoi diagram of four lines in general position in \mathbb{R}^3 can be obtained from one of these topologies by inserting full twists; each twist induces a bounded face of exactly two vertices in both the nearest and farthest diagrams. We obtain the classification by an exhaustive search algorithm using some new structural and combinatorial observations of line Voronoi diagrams.

2012 ACM Subject Classification Theory of computation → Computational geometry

Keywords and phrases Voronoi diagram, line, three dimensions, structural properties

Funding Supported by the Swiss National Science Foundation (SNF), project 200021E_201356

Acknowledgements We thank Dr. Martin Suderland for early discussions and valuable comments related to Sections 2, 3, and for two MATLAB-based visualisation tools, which allowed us to visualize $\Gamma(\text{FVD}(L))$, Fig. 8, and Fig. 24. We also thank SoCG anonymous reviewers for comments that helped improve the presentation of this paper, the general position assumption, and Lemma 3.

1 Introduction

Voronoi diagrams are fundamental space partitioning structures in Computational Geometry. Given a set S of n objects in some space, called sites, the *nearest* (respectively, *farthest*) Voronoi diagram of S decomposes the underlying space into regions that have the same nearest (resp., farthest) site. In this paper, we consider Voronoi diagrams of lines in \mathbb{R}^3 under the Euclidean metric, focusing on the elementary, yet fundamental base case of four lines.

The Euclidean Voronoi diagram of point sites in \mathbb{R}^d is a classical geometric partitioning structure that is generally well-understood. It has complexity $O(n^{\lceil \frac{d}{2} \rceil})$ and can be computed in $O(n \log n + n^{\lceil \frac{d}{2} \rceil})$ time [7, 10, 16]; these bounds are tight. The results also hold for certain polyhedral norms such as the L_∞ or L_1 norms [6, 15]. For the Euclidean farthest Voronoi diagram of point sites, exact worst-case bounds in the range of $\Theta(n^{\lceil \frac{d}{2} \rceil})$ have also been reported by Seidel [20].

For sites more general than points, however, Voronoi diagrams in \mathbb{R}^d , $d \geq 3$, have not yet been well-understood. These diagrams get complicated because their bisecting surfaces are curved, triggering complicated algebraic descriptions of their features such as their trisector curves. The combinatorial complexity of the classical Voronoi diagram of n lines (or line segments) in \mathbb{R}^3 is a well-known outstanding open problem [19]. There is a gap of an order

of magnitude between the $\Omega(n^2)$ lower bound [2] and the only known $O(n^{3+\epsilon})$ upper bound by Sharir [21]. This gap extends to the Voronoi diagram of lines in \mathbb{R}^d , $d > 3$, where the known upper bound is $O(n^{d+\epsilon})$ [21]. For $d \geq 4$, an $\Omega(n^{\lceil 2d/3 \rceil})$ lower bound has recently been reported by Glisse [13]. The upper bounds are derived from general complexity results on envelopes of algebraic functions in \mathbb{R}^{d+1} , under the general framework [10] for studying Voronoi diagrams in \mathbb{R}^d through the *arrangement* of distance functions of the given sites in \mathbb{R}^{d+1} . Sharper complexity bounds have been established in certain special cases such as lines with c constant orientations [18] and parallel half-lines [3], and for norms induced by convex polyhedra of constant complexity [4, 8, 17].

The Voronoi diagram of only three lines in \mathbb{R}^3 was addressed by the authors of [12] who proved the fundamental properties of its structure. The trisector of three pairwise skew lines was shown to consist of four unbounded curves, which are roots of a nonsingular quartic, or a nonsingular cubic and a nonintersecting line. This is the first, most basic building block necessary in computing any Voronoi diagram of lines or polyhedra in \mathbb{R}^3 , but it contains no Voronoi vertices. In this paper, we address the next basic building block, which is the Voronoi diagram of four lines in \mathbb{R}^3 , where a minimal number of Voronoi vertices appears.

The unbounded features of the Euclidean order- k , $1 \leq k \leq n-1$, Voronoi diagrams of lines and line segments in \mathbb{R}^d , $d \geq 3$, were studied in [5]. They are encoded in a map on a *sphere of directions*, called the Gaussian map, which has complexity $O(\min\{k, n-k\}n^{d-1})$; for the farthest Voronoi diagram the Gaussian map has complexity $\Theta(n^{d-1})$.

The Voronoi diagram of lines in \mathbb{R}^3 can be computed in $O(n^{3+\epsilon})$ time [1] as part of a more general technique to compute the lower envelope of algebraic functions in \mathbb{R}^4 . Using the envelope package of CGAL, a numerically robust algorithm for computing the Voronoi diagram of lines in \mathbb{R}^3 has been reported in [14]. Algorithms for computing approximations of the Voronoi diagram also exist, see e.g., [9, 11].

Contribution. In this paper, we prove structural properties of the Voronoi diagram of four lines in \mathbb{R}^3 , building upon the previous work [12] on three lines. The case of four lines is fundamental, and is required for understanding any Voronoi diagram of lines or polyhedra in \mathbb{R}^3 . We first show that the number of vertices in the Voronoi diagram of four lines in general position is always even, between 0 and 8, and all such numbers can be realized. We then identify basic structures in the arrangement of trisectors, called *twists*, which are critical for the formation of the diagram and the resulting number of its Voronoi vertices. A twist is a pair of consecutive trisector intersections along some trisector components (called branches, see Definition 11). We show that there are only two types of twists: *full twists* that involve four different trisector branches, and *partial twists* that involve six trisector branches, two of which are incident to both vertices of the twist (see Definition 12). A full twist has a *local* structure, in the sense that adding or removing one does not affect the rest of the diagram. It results in a bounded face with exactly two vertices in both the nearest and the farthest diagrams. Since full twists only have a local effect, we first assume that no full twists exist in the trisector arrangement, and fully classify the Voronoi diagrams of four lines in this case. We prove the following theorems.

► **Theorem 1.** *The Voronoi diagram of four lines in general position in \mathbb{R}^3 (both the nearest and farthest diagram) has 15 distinct topologies, assuming there are no full twists among the trisectors. The distinct topologies of the nearest and the farthest diagrams are in one-to-one correspondence. Further, they are in one-to-one correspondence with the unbounded features of the farthest diagram. To obtain more than two Voronoi vertices, twists are required. The two-dimensional faces in both diagrams are unbounded and the total number of vertices is at*

most 6, see Table 1. In the nearest Voronoi diagram, all vertices are connected in a single component of the 1-skeleton.

Number of vertices	0	2	4	6	8
Number of topologies	1	3	5	6	0

■ **Table 1** Distinct topologies for each possible number of Voronoi vertices, assuming no full twists.

Additional structural properties are listed in Observation 23.

► **Theorem 2.** *The nearest (resp. farthest) Voronoi diagram of four lines in general position in \mathbb{R}^3 can be obtained from one of the 15 topologies of Theorem 1 by inserting the diagram’s full twists. Inserting a full twist to a topology creates one new bounded face with two vertices in both the nearest and farthest diagram; it also splits an existing face in two faces. The total number of vertices, including full-twists, is at most 8.*

To obtain this classification, we devise an exhaustive search algorithm that enumerates possible *configurations* of projected trisector pairs. By ignoring the geometry and focusing on the structure, we encode a bisector and the two trisectors it contains as a *configuration* of eight curves in the plane, where each trisector has four branches. We identify necessary conditions under which a configuration is valid, and use them to create filters that eliminate impossible cases. We also create filters for six-tuples of configurations, where each tuple corresponds to the six bisectors of four lines. After an exhaustive search, which eliminates impossible cases by the derived necessary conditions, we are left with only 15 distinct configuration six-tuples. Each tuple is shown to correspond to a distinct topology and the enumeration process is shown to be complete. All 15 tuples and their corresponding topologies are realizable as we demonstrate by concrete examples. These results also provide an algebraically simple method to identify the structure of the Voronoi diagram.

In addition, we establish some simple new combinatorial results on the nearest and farthest Voronoi diagrams of n lines, expressing their features as a function of the number of Voronoi vertices (see Theorem 10). We use these results for $n = 4$ to obtain the aforementioned filters. For the farthest Voronoi diagram of n lines, we show that the region of each line has exactly $n-1$ three-dimensional cells, extending a result of [5] on the total number of cells.

The exhaustive search has been implemented as a program, available on GitHub [22], which performs the actual search.

2 Preliminaries

Let $L = \{\ell_1, \dots, \ell_n\}$ be a set of n lines in general position in \mathbb{R}^3 . By general position, we mean the following: (1) lines are pairwise skew, and no three lines are parallel to a common plane; (2) no sphere can be tangent to four lines with coplanar tangency points; (3) no sphere is tangent to five lines; (4) no four lines have direction vectors whose representations on the sphere of directions are cocircular.

We denote by $d(x, y)$ the Euclidean distance between two points $x, y \in \mathbb{R}^3$. The distance $d(x, \ell)$ from a point $x \in \mathbb{R}^3$ to a line $\ell \in L$ is defined as $d(x, \ell) = \min\{d(x, y) \mid y \in \ell\}$. The i -sector of i lines in \mathbb{R}^3 , $i \in \{2, 3\}$, is the locus of points equidistant from the i lines. For $i = 2$, a bisector $B(\cdot, \cdot)$ is a hyperbolic paraboloid; for $i = 3$, a trisector $T(\cdot, \cdot, \cdot)$ is a quartic consisting of four unbounded branches [12, 18]. Two trisectors are said to be *related* if they involve exactly four lines, i.e., they are of the form $T(\ell_i, \ell_j, \ell_k), T(\ell_i, \ell_j, \ell_l)$, with $k \neq l$.

The *nearest Voronoi diagram* of L , denoted $\text{NVD}(L)$, subdivides \mathbb{R}^3 into maximal regions, each consisting of points closer to one line than to any other line. More generally, for $1 \leq k \leq n-1$, the *order- k Voronoi diagram*, denoted $\text{VD}_k(L)$, subdivides \mathbb{R}^3 into maximal regions that have the same k nearest lines. The case $k = n-1$ gives the *farthest Voronoi diagram*, denoted $\text{FVD}(L)$. Each diagram is a 3D cell complex, whose *features* are vertices, edges, faces (2D), and cells (3D). Unless otherwise stated, we call 2D faces simply *faces* and 3D cells simply *cells*.

The general position assumptions imply the following properties. By assumption (1), the topology of trisectors is unique, [12] Theorem 1. By (2), related trisectors intersect transversely (see Lemma 3). By (3), vertices of the nearest and farthest Voronoi diagrams have degree 4. By (4), the asymptotes of related trisectors do not coincide (see Lemma 4).

► **Lemma 3.** *If two related trisectors (associated with four lines) intersect tangentially, then there exists a sphere tangent to the four lines such that the four contact points are coplanar.*

Proof. Assume that the related trisectors $T(\ell_1, \ell_2, \ell_3)$ and $T(\ell_1, \ell_2, \ell_4)$ intersect tangentially at point p . Let p_i denote the point on line ℓ_i , $i = 1, 2, 3, 4$, that is closest to p . Let v be a tangent direction of $T(\ell_1, \ell_2, \ell_3)$ at p ; then v is also a tangent direction of $T(\ell_1, \ell_2, \ell_4)$ at p . Since $T(\ell_1, \ell_2, \ell_3) = B(\ell_1, \ell_2) \cap B(\ell_1, \ell_3)$, the tangent direction v is parallel to $\vec{n}_1 \times \vec{n}_2$, where \vec{n}_1 (resp. \vec{n}_2) is the normal to $B(\ell_1, \ell_2)$ (resp. $B(\ell_1, \ell_3)$) at p . Similarly, v is parallel to $\vec{n}_1 \times \vec{n}_3$, where \vec{n}_3 is the normal to $B(\ell_1, \ell_4)$ at p . Since $B(\ell_1, \ell_2)$ bisects ℓ_1, ℓ_2 and p_1, p_2 are the closest points to p on ℓ_1 and ℓ_2 , we have $\vec{n}_1 \parallel \vec{p_1 p_2}$. Similarly, $\vec{n}_2 \parallel \vec{p_1 p_3}$ and $\vec{n}_3 \parallel \vec{p_1 p_4}$. Hence, the four points p_1, p_2, p_3, p_4 are coplanar. This completes the proof. ◀

For a cell complex M , let B be a ball large enough to intersect any i -dimensional feature of M , for $0 \leq i \leq 3$, in one connected component. Let Γ be the boundary of B . The intersection $M \cap \Gamma$ encodes the unbounded features of M into a two-dimensional map on Γ , denoted $\Gamma(M)$. In particular, the unbounded edges, unbounded 2D faces, and unbounded 3D cells of M correspond exactly to the vertices, edges and faces, respectively, of $\Gamma(M)$.

Next, we give a summary of known elementary properties for the Voronoi diagram of four lines. Four lines induce four trisectors and six bisectors. When two trisectors intersect, the other two trisectors necessarily pass through the same intersection points. These intersections are Voronoi vertices in the order- k Voronoi diagram, $k \in \{1, 2, 3\}$. Voronoi vertices lie on all six bisectors. A trisector consists of four unbounded curves, called branches. Trisector branches are partitioned by the Voronoi vertices into arcs, which are order- k Voronoi edges for some k . Each trisector lies in three bisectors, and each bisector contains exactly two trisectors. A bisector is partitioned by the two trisectors it contains into faces, where each face belongs to an order- k Voronoi diagram, for some k . The nearest and farthest Voronoi diagrams of four lines share no edges or faces, by definition. In contrast, both diagrams share their edges with the order-2 Voronoi diagram.

2.1 Algebraic framework and geometric reinterpretation

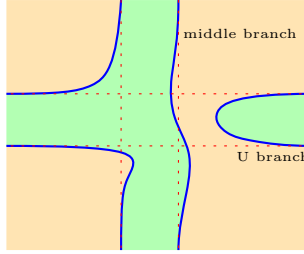
We recall the parametrization of lines from [12]. WLOG, let the coordinate system satisfy the following: ℓ_1 is defined by point $(0, 0, 1)$ and vector $(1, a, 0)$, ℓ_2 is defined by point $(0, 0, -1)$ and vector $(1, -a, 0)$, for some $a \in \mathbb{R}$. For $i \geq 3$, line ℓ_i is defined by point $(b_i, c_i, 0)$ and vector $(d_i, e_i, 1)$, with $b_i, c_i, d_i, e_i \in \mathbb{R}$. Then, the bisector $B(\ell_1, \ell_2)$ has the following formulation:

$$B(\ell_1, \ell_2) = \{(x, y, z) \mid (x, y) \in \mathbb{R}^2, z = \frac{-a}{1+a^2} \cdot xy\}.$$

There is a natural homeomorphism $\Pi : B(\ell_1, \ell_2) \rightarrow \mathbb{R}^2$, given by $\Pi(x, y, z) = (x, y)$, that projects the bisector onto the Euclidean plane. We call $\Pi(B(\ell_1, \ell_2))$ the *projected bisector*. For any trisector $T = T(\ell_1, \ell_2, \ell_i)$ on $B(\ell_1, \ell_2)$, we call $\Pi(T)$ the *projected trisector*. The following lemma summarizes key properties of the Voronoi diagram of three lines from [12], including [12] Propositions 14 and 17. We restate them in the following lemma in terms of projected trisectors on projected bisectors, as needed for analyzing four lines in Sections 4 and 5. Refer to Fig. 1.

► **Lemma 4** ([12]). *A projected trisector T consists of four unbounded branches. It has two vertical and two horizontal asymptotes. There is a unique branch that admits exactly one asymptote, called the middle branch. The middle branch partitions a projected bisector into two regions: one containing a single branch and the other containing two branches; denote the single branch as the U branch. Furthermore, the following hold:*

1. *the middle branch of T is the same on all three bisectors that T lies on;*
2. *the three branches of T , other than the middle branch, each becomes a U branch on exactly one of the three bisectors that T lies on;*
3. *the four branches of T partition the bisector into five faces, two of which belong to the NVD and three belong to the FVD of the three lines;*
4. *if the asymptote of the middle branch is vertical, then all branches are y -monotone; otherwise, all branches are x -monotone.*



■ **Figure 1** A projected trisector on a projected bisector. Branches are shown in blue and the asymptotes are shown in red. The NVD faces are shown in green and the FVD faces in orange.

3 Some combinatorial results on Voronoi diagrams of lines in \mathbb{R}^3

We first analyze the asymptotes of a projected trisector, building upon the results of [12]. The following lemma uses the parametrization notation of Section 2.1.

► **Lemma 5.** *The vertical and horizontal asymptotes of a projected trisector $\Pi(T(\ell_1, \ell_2, \ell_i))$, on the projected bisector $\Pi(B(\ell_1, \ell_2))$, are roots of quadratic polynomials whose coefficients depend only on the parameters a, d_i, e_i that define the direction of the line ℓ_i . Consequently, the asymptotes of the projected trisector are invariant under translation of the line ℓ_i .*

Proof. Let $p = (x, y, z)$ be a point on $T = T(\ell_1, \ell_2, \ell_i)$; then $d(p, \ell_1) = d(p, \ell_2)$ and $d(p, \ell_1) = d(p, \ell_i)$. The first equation yields $z = -\frac{a}{1+a^2}xy$, by our choice of coordinates. We substitute this expression for z in the second equation. Consequently, the projection of T onto the xy -plane satisfies $P(x, y) := A(x)y^2 + B(x)y + C(x) = 0$, where $A(x), B(x), C(x)$ are quadratic in x with coefficients depending on a, b_i, c_i, d_i, e_i . The explicit expressions are: $A(x) = a^2 + a^4 + a^2d_i^2 + a^4d_i^2 - e_i^2 - a^2e_i^2 + 2ae_ix + 2a^3e_ix - a^2x^2$, $B(x) = -2c_i - 4a^2c_i - 2a^4c_i - 2c_id_i^2 - 4a^2c_id_i^2 - 2a^4c_id_i^2 + 2b_id_ie_i + 4a^2b_id_ie_i + 2a^4b_id_ie_i - 2ab_id_ix - 2a^3b_id_ix - 2ac_ie_ix - 2a^3c_ie_ix -$

$2d_i e_i x - 4a^2 d_i e_i x - 2a^4 d_i e_i x + 2ad_i x^2 + 2a^3 d_i x^2$, and $C(x) = -1 - 2a^2 - a^4 + c_i^2 - d_i^2 - 2a^2 d_i^2 - a^4 d_i^2 + c_i^2 d_i^2 + 2a^2 c_i^2 (1 + d_i^2) + a^4 c_i^2 (1 + d_i^2) - 2b_i c_i d_i e_i - 4a^2 b_i c_i d_i e_i - 2a^4 b_i c_i d_i e_i - e_i^2 - 2a^2 e_i^2 - a^4 e_i^2 + b_i^2 (1 + e_i^2) + 2a^2 b_i^2 (1 + e_i^2) + a^4 b_i^2 (1 + e_i^2) - 2b_i x - 4a^2 b_i x - 2a^4 b_i x + 2c_i d_i e_i x + 4a^2 c_i d_i e_i x + 2a^4 c_i d_i e_i x - 2b_i e_i^2 x - 4a^2 b_i e_i^2 x - 2a^4 b_i e_i^2 x + x^2 + a^2 x^2 - a^2 d_i^2 x^2 - a^4 d_i^2 x^2 + e_i^2 x^2 + a^2 e_i^2 x^2$.

Any real vertical asymptote $x = x_0$ must satisfy $A(x_0) = 0$. The coefficients of $A(x)$ are polynomials in a, d_i, e_i , which depend solely on the directions of the lines. Similarly, $P(x, y)$ can also be expressed as $A'(y)x^2 + B'(y)x + C'(y)$, where $A'(y), B'(y), C'(y)$ are quadratic in y with coefficients depending on a, b_i, c_i, d_i, e_i . Any real horizontal asymptote $y = y_0$ must satisfy $A'(y_0) = 0$, where $A'(y) = -a^4 d_i^2 + 2a^3 d_i y - a^2 d_i^2 + a^2 e_i^2 - a^2 y^2 + a^2 + 2ad_i y + e_i^2 + 1$, whose coefficients depend solely on the directions of the lines. This completes the proof. \blacktriangleleft

The number of vertices in the Voronoi diagram of four lines is known to be at most 8 [18]. We extend this observation and show that the number of vertices is always even.

► Lemma 6. *The number of vertices in a Voronoi diagram of four lines in general position is always even, between 0 and 8, and all numbers can be attained.*

Proof. By the general position assumption, item (4), related trisectors have different asymptotes. This is because, if two related trisectors have the same asymptote, then the four corresponding direction vectors have cocircular representations on the sphere of directions (with the center of the circle being the direction of the asymptote). Since Voronoi vertices appear on all six bisectors, it suffices to show that the number of vertices on one projected bisector is even. All calculations are modulo 2.

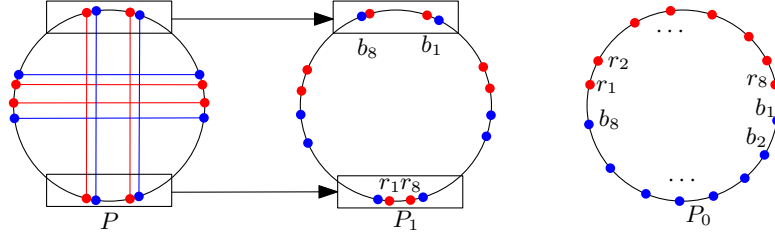
Consider a projected bisector with two projected trisectors colored red and blue. Consider a large circle C . Let $r_1, \dots, r_8, b_1, \dots, b_8$ be the intersection points of the red and blue projected trisectors with C . Let C be large enough so that the order of these points on C is the same as the order of the intersections between C and the asymptotes of the projected trisectors. Let P be the circular order of the points. We name the red points corresponding to one trisector branch r_{2i-1} and r_{2i} , for $i \in \{1, 2, 3, 4\}$; similarly for the blue points.

Consider a red branch with endpoints r_1, r_2 and a blue branch with endpoints b_1, b_2 . Then, these two branches intersect precisely k times, where k is the number of blue endpoints that are between r_1 and r_2 in P (recall that calculation is under modulo 2). Summing over all blue branches, the number of vertices on this red branch equals the number of blue endpoints between r_1 and r_2 in P . Denote this number by $x_{1,2}$. Hence, the total number of vertices is $x = x_{1,2} + x_{3,4} + x_{5,6} + x_{7,8}$.

We make the following observation: if a red point and an adjacent blue point are swapped in P , x changes by 1. When $P_0 = \{r_1, \dots, r_8, b_1, \dots, b_8\}$, we have $x = 0$ (note that P_0 cannot be realized by real projected trisectors, but our proof does not depend on it). It suffices to show that any given order P can be transformed to P_0 by an even number of swaps. We show this through an intermediate step P_1 defined in Fig. 2. One can check that in 12 swaps, one can move b_1, b_8, r_1, r_8 from their positions in P_0 to those in P_1 . Hence, it remains to show that any order P given by two related trisectors can be transformed to P_1 by an even number of swaps.

By symmetry of the vertical asymptotes, we can see that the number of swaps needed for the top four points is the same as the number of swaps needed for the bottom four points, in order to transform from P to P_1 . Similarly for the left and right points that correspond to the horizontal asymptotes. Hence, the total number of swaps from P to P_1 is even.

It was shown by Koltun and Sharir [18] that the Voronoi diagram of four lines has at most 8 vertices. For all even numbers between 0 and 8, there are lines in general position that give the corresponding number of vertices. See Appendix A for examples with vertices between 0 and



■ **Figure 2** Illustration for the proof of Lemma 6.

6. The following parameters $(a, b_3, c_3, d_3, e_3, b_4, c_4, d_4, e_4) = (10, 14, -6, -9, -5, -19, 5, 13, 11)$ give four lines that have 8 Voronoi vertices, which can be verified numerically by showing that the system of equations $d(p, \ell_1) = d(p, \ell_i)$, for $i \in \{2, 3, 4\}$ and $p \in \mathbb{R}^3$, has exactly 8 real roots. This completes the proof. ◀

► **Remark 7.** Following the discussion in Section 5.2, a simpler proof can be obtained as follows. The number of Voronoi vertices equals the number of intersections of two projected trisectors on a projected bisector, which is captured by a configuration. If a configuration has no twists, i.e., if every pair of branches intersect at most once, then such a configuration is “simple”, see Step 1 in Phase 1. All simple configurations are generated by the exhaustive search algorithm, and they all have an even number of intersections. Any other configuration differs from its corresponding simple configuration by an even number of intersections. This completes the alternative proof.

The farthest Voronoi diagram of a set L of n lines in general position is known to have $n^2 - n$ distinct 3D cells, which are all unbounded, and do not form tunnels [5]. The following lemma follows from [5] and extends this result to the cells of individual lines.

► **Lemma 8.** *In the farthest Voronoi diagram of n lines in general position, $n \geq 2$, the Voronoi region of each line consists of exactly $n-1$ unbounded 3D cells.*

Proof. The argument follows the proofs of [5] Theorems 5.11 and 5.12, together with the following observation. For a line ℓ_i , consider the set of directions on the unit sphere \mathbb{S} orthogonal to ℓ_i . These directions form a great circle C_i . Consider C_1 , which intersects each other great circle C_i in exactly two points, at the “vertices of anomaly” (as defined in [5]). These two points are antipodal. For each pair of vertices of anomaly, exactly one point separates a face of ℓ_1 in $\Gamma(\text{FVD}(L))$, and the other separates a face of ℓ_i in $\Gamma(\text{FVD}(L))$. Hence, C_1 is divided into exactly $n-1$ arcs. The remaining steps proceed as in the proof of Theorem 5.12 in [5]. ◀

In $\text{NVD}(L)$, where L is a set of n lines in general position, 3D Voronoi regions are connected, and each region is topologically an infinite cylinder with two unbounded ends, assuming $n \geq 3$. Thus, we can derive the following results for $\text{NVD}(L)$. The farthest counterpart follows from [5] Theorem 5.12.

► **Lemma 9.** *The map $\Gamma(\text{NVD}(L))$ has $4n-4$ vertices, $6n-6$ edges, and $2n$ faces. The map $\Gamma(\text{FVD}(L))$ has $2n^2-2n-4$ vertices, $3n^2-3n-6$ edges, and n^2-n faces. The numbers indicate the unbounded Voronoi edges, faces, and cells, respectively, in each diagram.*

Proof. By the general position assumption, item (4), each vertex in the unbounded map $\Gamma(\text{NVD}(L))$ (resp. $\Gamma(\text{FVD}(L))$) is incident to exactly three edges, and each edge is incident to two vertices. There are n 3D cells in $\text{NVD}(L)$, each of which is an infinite topological

cylinder with two unbounded ends. Hence, $\Gamma(\text{NVD}(L))$ has $2n$ faces. By [5] Theorem 5.12, $\Gamma(\text{FVD}(L))$ has $n^2 - n$ faces. Both $\Gamma(\text{NVD}(L))$ and $\Gamma(\text{FVD}(L))$ are planar graphs, so Euler's formula applies. The stated results then follow easily. ◀

Note that the *Gaussian map* on the sphere of directions from [5] can be regarded as the limit of the unbounded features map on Γ , as Γ goes to infinity. Combining Lemma 9 and some counting arguments, we derive the following result, which we use for $n = 4$ in Section 5.

- **Theorem 10.** *Let V_N (resp. V_F) denote the number of vertices of NVD(L) (resp. FVD(L)).*
- *NVD(L) has $2V_N + 2n - 2$ edges, $V_N + 3n - 3$ faces, and n cells.*
 - *FVD(L) has $2V_F + n^2 - n - 2$ edges, $V_F + 2n^2 - 2n - 3$ faces, and $n^2 - n$ cells.*

Proof. Let V , E , and F denote the numbers of vertices, edges, and faces of the diagram under consideration.

Consider the NVD(L). For a 3D cell c , let V_c, E_c, F_c be the numbers of vertices, edges, and faces of c . Since c is an infinite topological cylinder with two unbounded ends, its intersection with the large sphere Γ consists of two disjoint faces. Consequently, Euler's formula yields the equation $V_c - E_c + F_c = 0$. Summing over all 3D cells of NVD(L) yields $4V - 3E + 2F = 0$, since each vertex/edge/face is incident to 4/3/2 cells.

Let E_0, E_1, E_2 be the numbers of edges that are incident to two vertices, incident to one vertex, and not incident to any vertex, respectively. By counting the vertex-edge-incidences, we get $2E_0 + E_1 = 4V$. By Lemma 9, we get $E_1 + 2E_2 = 4n - 4$. Combining with $E = E_0 + E_1 + E_2$ gives $E = 2V + 2n - 2$ and $F = V + 3n - 3$.

Now consider FVD(L). Each 3D cell c corresponds to a single face of $\Gamma(\text{FVD}(L))$ [5]. Similarly, Euler's formula gives the equation $V_c - E_c + F_c = 1$. Summing up over the $n^2 - n$ 3D cells of FVD(L) yields $4V - 3E + 2F = n^2 - n$. The rest of the proof is similar to NVD(L). Finally, we get $E = 2V + n^2 - n - 2$ and $F = V + 2n^2 - 2n - 3$. ◀

4 Twists

From this section onward, we focus on a set L of four lines in general position. The four lines give rise to four trisectors that form the trisector system of L , and six bisectors.

► **Definition 11.** *A pair of trisector intersections (v_1, v_2) is called a twist, if there exist two trisectors T_1, T_2 , that both have a single branch passing through v_1, v_2 consecutively (i.e., no other vertices exist between v_1 and v_2 on either T_1 or T_2); see Fig. 3.*

► **Definition 12.** *A twist (v_1, v_2) is called a full twist, if there are exactly four trisector branches passing through v_1 and v_2 consecutively (with no other vertices between v_1, v_2 on any branch); see Fig. 3 right. A twist is called a partial twist, if there are exactly two trisectors with a single branch passing through both v_1 and v_2 , and two trisectors with exactly two branches each, one passing through v_1 and the other through v_2 ; see Fig. 3 left.*



■ **Figure 3** Left: a partial twist. Right: a full twist. Different colors denote different trisectors.

The proof of the following lemma is deferred to the next section.

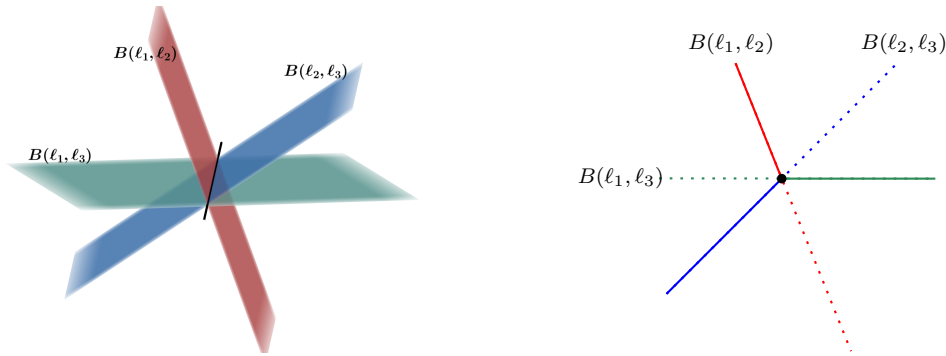
► **Lemma 13.** *A twist is either a full twist or a partial twist.*

4.1 Full twists

We show that the Voronoi diagram (both nearest and farthest) exhibits a unique local structure around any full twist; see Fig. 5 for an illustration.

► **Lemma 14.** *Among the four bounded trisector arcs incident to a full twist, exactly two lie in $NVD(L)$ and the other two lie in $FVD(L)$, defining one bounded face in each diagram called a full-twist face. The arcs alternate between the nearest and the farthest diagrams, alternate in the sense that the two full-twist faces intersect each other.*

Proof. Consider a local section of the trisector $T(\ell_1, \ell_2, \ell_3)$. It is the intersection of three bisectors, $B(\ell_1, \ell_2)$, $B(\ell_1, \ell_3)$, and $B(\ell_2, \ell_3)$, which intersect transversely [12]. Around this local section, the NVD and FVD portions of the bisectors alternate, following exactly the structure shown in Fig. 4.

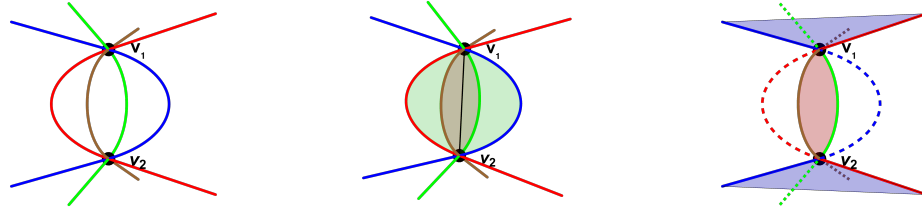


■ **Figure 4** Left: the three bisectors intersect transversely. Right: view along the trisector; solid rays indicate the NVD portions, dotted rays indicate FVD portions. The rays that belong to the NVD and the FVD alternate when rotating around the center.

Let (v_1, v_2) be a full twist, see Fig. 5. Since the incident trisector arcs are all related, each pair of them bounds a bisector face in $VD_k(L)$ for some k , $1 \leq k \leq 3$. We will show that two of the incident trisectors arcs belong to $NVD(L)$, and two belong to $FVD(L)$; furthermore, they alternate.

Assume for the sake of contradiction that at least three of the trisector arcs incident to v_1, v_2 belong to $NVD(L)$ (resp. $FVD(L)$). Then the three bounded arcs give rise to three bounded faces in $NVD(L)$ (resp. $FVD(L)$), which together form a bounded 3D cell in $NVD(L)$ (resp. $FVD(L)$). This contradicts the fact that the 3D cells of these diagrams are unbounded.

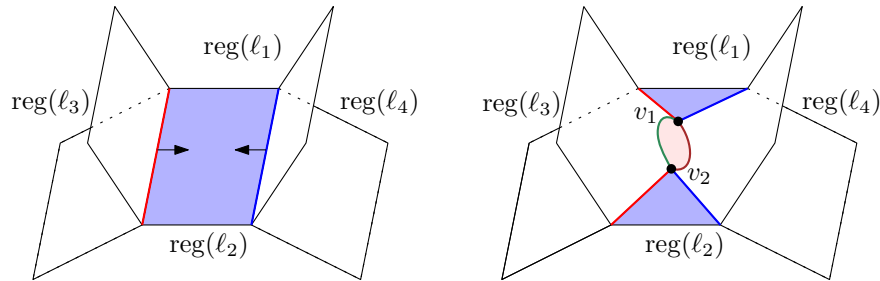
Hence, among the four bounded arcs incident to the full twist vertices, exactly two arcs belong to $NVD(L)$, defining an NVD face, and two belong to $FVD(L)$, defining an FVD face. Assume for the sake of contradiction that the NVD and FVD arcs do not alternate; wlog, let the red and green arcs be in $NVD(L)$ and the other two arcs be in $FVD(L)$, see Fig. 5 left. Consider the face F_1 (resp. F_2) bounded by the red and blue (resp. green and brown) arcs in Fig. 5 middle. Both faces belong to $VD_2(L)$ since they are incident to both NVD and FVD edges. The two faces F_1, F_2 intersect at a curve that is not an edge of the diagram (which can be proven formally using the fact that related bisectors intersect transversely), see Fig. 5 middle, deriving a contradiction. ◀



■ **Figure 5** Left: a 3D view of a full twist. Middle: illustration for the proof of Lemma 14. Faces F_1 and F_2 are highlighted, intersecting at the black segment which is not an edge of the diagram. Right: the unique structure of the $\text{NVD}(L)$ around the full twist.

The converse of the above lemma is also true, which will be shown in Lemma 17. Next, we describe a local modification on a Voronoi diagram associated with a full twist.

Local modification. Refer to Fig. 6. Start with an NVD face incident to two edges from different trisectors (e.g., the blue face on $B(\ell_1, \ell_2)$ incident to the red and blue edges). Move the interior of the edges closer until they intersect twice (at vertices v_1, v_2). Consequently, each of the two original edges is split into three pieces, and the middle arcs no longer belong to the NVD. The original NVD face is split into two faces. Two new bounded edges from the other two trisectors appear in the diagram (the green and brown edges in Fig. 6), which form a full-twist face in the NVD. The cells of ℓ_3 and ℓ_4 touch each other along the full-twist face. The local modification applies to the FVD in the same way.



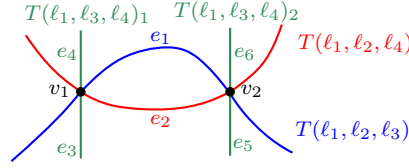
■ **Figure 6** Left: local NVD/FVD structure; right: the modified diagram after adding a full twist.

We say that the diagram in Fig. 6 right is obtained from the diagram in Fig. 6 left by “adding a full twist”. The local operation can be reversed by “removing a full twist”. Since the effect of a full twist is purely local, we first focus on the global structure, by restricting attention to Voronoi diagrams whose trisector arrangements have no full twists.

4.2 Partial twists and further properties

We illustrate the local structure of the Voronoi diagrams around twists, and prove that any twist in the trisector arrangement must be either full or partial.

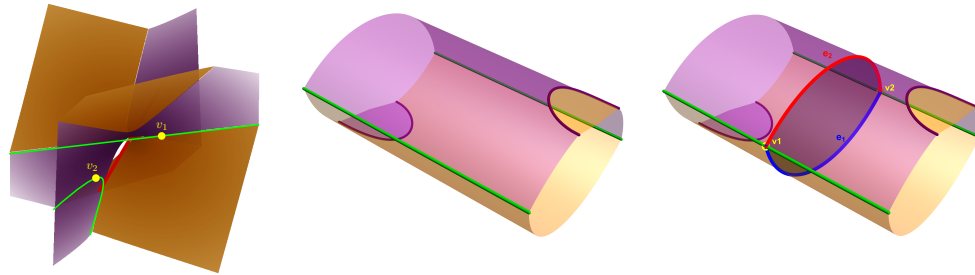
► **Lemma 15.** *Let (v_1, v_2) be a twist and let (e_1, e_2) be the two trisector arcs incident to both v_1, v_2 , as shown in Fig. 7. Assume that a third trisector has two distinct branches, one of which passes through v_1 and the other through v_2 . Then, one of e_1, e_2 belongs to $\text{NVD}(L)$ and the other belongs to $\text{FVD}(L)$; the face bounded by e_1, e_2 belongs to $\text{VD}_2(L)$.*



■ **Figure 7** A local section of a trisector system, illustrating the setup of Lemma 15.

Proof. Refer to Fig. 7. We distinguish two branches of trisector $T(\ell_1, \ell_3, \ell_4)$ as $T(\ell_1, \ell_3, \ell_4)_1$ and $T(\ell_1, \ell_3, \ell_4)_2$. Note that one of the edges e_3, e_4 in $T(\ell_1, \ell_3, \ell_4)_1$ is an NVD edge and the other is an FVD edge. Analogously for the edges e_5, e_6 in $T(\ell_1, \ell_3, \ell_4)_2$. Hence, wlog, we assume that e_4, e_6 are edges of $\text{NVD}(L)$.

Assume for the sake of contradiction that e_1, e_2 are both in $\text{NVD}(L)$. Then, the face on $B(\ell_1, \ell_2)$ bounded by e_1 and e_2 is also in $\text{NVD}(L)$. Further, there is a face of $\text{NVD}(L)$ on $B(\ell_1, \ell_3)$ incident to e_1, e_4, e_6 , and a face of $\text{NVD}(L)$ on $B(\ell_1, \ell_4)$ incident to e_2, e_4, e_6 . Hence, there are two faces f_1 and f_2 in $\text{NVD}(\{\ell_1, \ell_3, \ell_4\})$, on $B(\ell_1, \ell_3)$ and $B(\ell_1, \ell_4)$, respectively, that are incident to both branches $T(\ell_1, \ell_3, \ell_4)_1$ and $T(\ell_1, \ell_3, \ell_4)_2$. By [12], the Voronoi region of a line in the NVD of three lines is invariant, which is shown schematically in Fig. 8-middle. To satisfy the aforementioned properties, faces f_1 and f_2 must be the top and bottom faces in Fig. 8-middle, and the two branches $T(\ell_1, \ell_3, \ell_4)_1$ and $T(\ell_1, \ell_3, \ell_4)_2$ must be the green branches in the same figure. Adding line ℓ_2 to $\text{NVD}(\{\ell_1, \ell_3, \ell_4\})$ creates vertices v_1, v_2 on the branches illustrated by green in Fig. 8-right, with incident edges e_1, e_2 on the top and bottom faces, and a face bounded by e_1, e_2 in $\text{NVD}(L)$, see Fig. 8-right. This new face splits the 3D cell of ℓ_1 into two components, which gives a contradiction as the 3D cells of $\text{NVD}(L)$ are topological infinite cylinders.



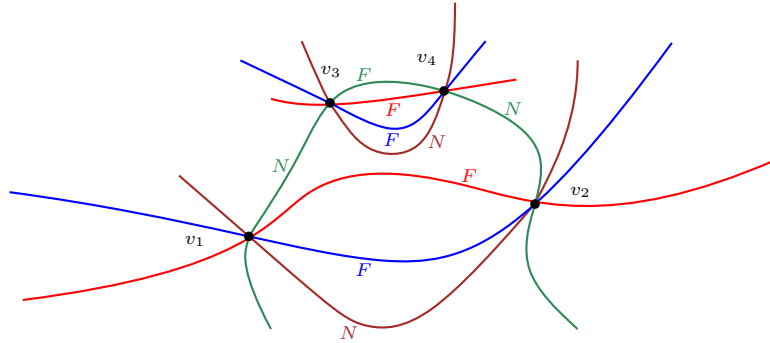
■ **Figure 8** The region of ℓ_1 in $\text{NVD}(\ell_1, \ell_3, \ell_4)$, with the two green trisector branches highlighted. Left: a real instance. Middle: a schematic representation. The purple faces belong to $B(\ell_1, \ell_4)$ and the yellow faces belong to $B(\ell_1, \ell_3)$. Right: the result of inserting ℓ_2 .

Next, assume that e_1, e_2 are both in $\text{FVD}(L)$. Analogously, we can show that there are two faces in $\text{FVD}(\{\ell_1, \ell_3, \ell_4\})$, on $B(\ell_1, \ell_3)$ and $B(\ell_1, \ell_4)$, respectively, that are incident to both trisector branches $T(\ell_1, \ell_3, \ell_4)_1$ and $T(\ell_1, \ell_3, \ell_4)_2$. However, such a pair of trisector branches does not exist, by Lemma 4 (items 2 and 3). Thus, one of e_1, e_2 is an NVD edge and the other is an FVD edge. Consequently, the face bounded by e_1 and e_2 lies in $\text{VD}_2(L)$. ◀

► **Corollary 16.** *For any partial twist, the face bounded by the two trisector arcs incident to both vertices of the partial twist belongs to the order-2 Voronoi diagram $\text{VD}_2(L)$.*

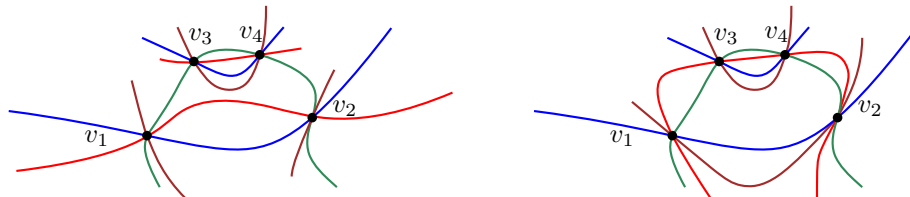
We can now use Lemma 15 to prove Lemma 13.

Proof of Lemma 13. Let (v_1, v_2) be a twist and assume for the sake of contradiction that it is neither partial nor full. Suppose that three trisector branches pass through v_1, v_2 consecutively. Since (v_1, v_2) is not a full twist, the fourth trisector T_4 , must either have (a) two branches through v_1 and v_2 , or (b) a single branch through v_1 and v_2 without v_1, v_2 being consecutive. In case (a) (Fig. 11 left), by the pigeonhole principle, at least two of the three bounded edges incident to the twist must lie in $\text{NVD}(L)$ or in $\text{FVD}(L)$, and this contradicts Lemma 15. Thus case (a) cannot occur. For case (b) we refer to the trisectors by their colors in Fig. 9 and show that case (b) cannot occur either.



■ **Figure 9** Labeling of the trisector system for type (b) in the proof of Lemma 13. The label ‘N’ (resp. ‘F’) on an edge indicates an NVD (resp. FVD) edge.

Consider the green trisector in Fig. 9 that has two vertices v_3 and v_4 between v_1 and v_2 . Then v_3 and v_4 must lie on the same red (resp. blue and brown) trisector branch, otherwise that trisector would self-intersect. Hence, the trisector system matches Fig. 9 (ignoring the edge labels for now). Consider the two bounded green arcs (v_1, v_3) and (v_2, v_4) . They belong to the same diagram (either NVD or FVD) since they are both incident to the green arc (v_3, v_4) . Assume that they are both NVD edges. Then the green arc (v_3, v_4) is an FVD edge. By the same reasoning as in the proof of Lemma 14, among the three bounded arcs incident to v_1 and v_2 (red, blue, and brown arcs), two belong to $\text{FVD}(L)$ and one belongs to $\text{NVD}(L)$. WLOG, let the brown arc belong to $\text{NVD}(L)$ and the blue, red arcs belong to $\text{FVD}(L)$. Consider the bisector containing the green and blue trisectors, and the bounded face with vertices v_1, v_3, v_4, v_2 . Since the face is bounded by edges from both $\text{NVD}(L)$ and $\text{FVD}(L)$, it is a VD_2 face. Hence, the blue edge (v_3, v_4) is an FVD edge. Similarly, the red edge (v_3, v_4) is an FVD edge. The four bounded edges incident to (v_3, v_4) contradict Lemma 14, since three of them lie in $\text{FVD}(L)$. The case where (v_1, v_3) and (v_2, v_4) are both FVD edges is analogous. Hence, case (b) cannot occur.

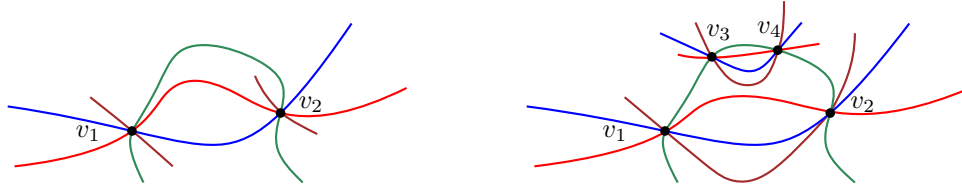


■ **Figure 10** Additional impossible cases.

Some additional cases are shown in Fig. 10. They can all be shown impossible using the same proof idea (inspecting the labels of edges on different faces). This completes the

proof. ◀

Case (b) of the above proof shows that “nested full twists”, as shown in Fig. 11 right, are impossible. Consequently, full twists are either isolated or sequential.



■ **Figure 11** Left: a trisector system corresponding to (a) in the proof of Lemma 13. Right: two “nested full twists”, corresponding to (b) in the proof of Lemma 13. Both are impossible.

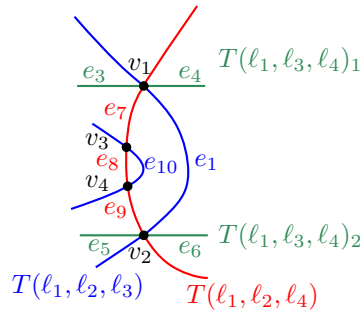
► **Lemma 17.** *In $NVD(L)$ (resp. $FVD(L)$), if there is a bounded face with exactly two edges and two vertices, then these vertices belong to a full twist.*

Proof. If the two bounded edges both lie in $NVD(L)$ (resp. $FVD(L)$), then each of the remaining two trisectors (other than those of the two edges) must have exactly one branch passing through the two vertices, by Lemma 15. If both remaining branches pass through the two vertices consecutively, then these vertices form a full twist. Otherwise, for at least one of the branches, there is an even number of vertices between the two vertices of the twist, which contradicts Lemma 13. ◀

Lemma 17 provides a concrete criterion to detect full twists by inspecting two projected trisectors (on a single bisector). It is used to classify Voronoi diagrams without full twists.

We finish the section with another technical lemma that generalizes Lemma 15. Its proof uses similar ideas to Lemma 15.

► **Lemma 18.** *Assume that related trisectors interact as shown in Fig. 12. Then one of the edges e_1 and e_7 belongs to $NVD(L)$ and the other belongs to $FVD(L)$. Consequently, the bounded face on $B(\ell_1, \ell_2)$ incident to v_1, v_3, v_4, v_2 belongs to $VD_2(L)$, and the vertices v_3, v_4 form a full twist.*



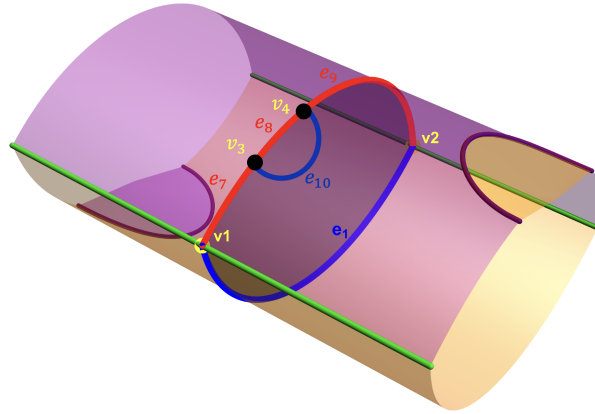
■ **Figure 12** A local trisector arrangement for Lemma 18.

Proof. For simplicity, we refer to the trisectors by their colors in Fig. 12. Assume to the contrary that e_1 and e_7 (and thus e_9 as well) both belong to $NVD(L)$ (resp. $FVD(L)$). Similarly to the proof of Lemma 15, there is a face of $NVD(\{\ell_1, \ell_3, \ell_4\})$ (resp. $FVD(\{\ell_1, \ell_3, \ell_4\})$)

on $B(\ell_1, \ell_3)$ that is incident to both trisector branches $T(\ell_1, \ell_3, \ell_4)_1$ and $T(\ell_1, \ell_3, \ell_4)_2$. We claim that on bisector $B(\ell_1, \ell_4)$, the two trisector branches $T(\ell_1, \ell_3, \ell_4)_1$ and $T(\ell_1, \ell_3, \ell_4)_2$ do not bound a common face in $\text{NVD}(\{\ell_1, \ell_3, \ell_4\})$ (resp. $\text{FVD}(\{\ell_1, \ell_3, \ell_4\})$).

Assume to the contrary that they do. For the FVD, the claim can be shown following the same logic as in the proof of Lemma 15: such a pair of trisector branches $T(\ell_1, \ell_3, \ell_4)_1$ and $T(\ell_1, \ell_3, \ell_4)_2$ does not exist, by Lemma 4 (items 2 and 3).

For the NVD, we can also use a similar idea as in the proof of Lemma 15: such a pair of trisector branches can only be the two green branches shown in Fig. 13, because of the unique structure of the Voronoi diagram of three lines [12]. Consider $\text{NVD}(L)$ as the result of adding line ℓ_2 to the $\text{NVD}(\{\ell_1, \ell_3, \ell_4\})$, which creates new vertices and edges shown in Fig. 13. Consider the face f bounded by e_8 and e_{10} on $B(\ell_1, \ell_2)$. By inspecting the bisector $B(\ell_1, \ell_2)$ with the red and blue trisectors in Fig. 12, it follows that every point in the interior of f is closest to ℓ_3 . However, this face f is contained in the cell of ℓ_1 in $\text{NVD}(\{\ell_1, \ell_3, \ell_4\})$. This gives a contradiction.



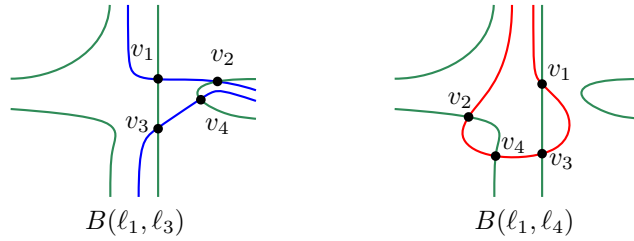
■ **Figure 13** Illustration for the proof of Lemma 18: a schematic 3D view of the cell of ℓ_1 in $\text{NVD}(\{\ell_1, \ell_3, \ell_4\})$ with some additional edges and vertices. The purple faces belong to $B(\ell_1, \ell_4)$ and the yellow faces belong to $B(\ell_1, \ell_3)$.

We have shown that the two green branches $T(\ell_1, \ell_3, \ell_4)_1$ and $T(\ell_1, \ell_3, \ell_4)_2$ bound a common FVD face on $B(\ell_1, \ell_3)$, but not on $B(\ell_1, \ell_4)$. For the remaining proof, we assume that both e_1 and e_7 are edges of $\text{FVD}(L)$. The case of $\text{NVD}(L)$ can be shown analogously. By Lemma 4, item 3, on $B(\ell_1, \ell_3)$, there is only one FVD face that is bounded by two distinct trisector branches, namely the middle branch and the U branch. Thus, the two green branches $T(\ell_1, \ell_3, \ell_4)_1$ and $T(\ell_1, \ell_3, \ell_4)_2$ are the middle and U branch respectively on $B(\ell_1, \ell_3)$. By Lemma 4 again, the bisector configurations of $B(\ell_1, \ell_3)$ and $B(\ell_1, \ell_4)$ are partially depicted in Fig. 14.

Consider the fourth trisector $T(\ell_2, \ell_3, \ell_4)$. It must have two different branches passing through v_1 and v_3 (otherwise by Lemma 13, v_1 and v_3 form a full twist which is a contradiction). Similarly, $T(\ell_2, \ell_3, \ell_4)$ must have two different branches passing through v_2 and v_4 , and two different branches passing through v_3 and v_4 . By Lemma 4 (items 1 to 3), it is not hard to see that such branches cannot exist.

Consequently, one of the edges e_1 and e_7 belongs to $\text{NVD}(L)$ and the other belongs to $\text{FVD}(L)$. The face on $B(\ell_1, \ell_2)$ bounded by v_1, v_3, v_4, v_2 is incident to both e_1 and e_7 , therefore it belongs to $\text{VD}_2(L)$. Hence, the face on $B(\ell_1, \ell_2)$ bounded by e_8 and e_{10} either belongs to $\text{NVD}(L)$ or $\text{FVD}(L)$. In either case, it implies that the vertices v_3 and v_4 form a

full twist, by Lemma 17. This completes the proof. ◀



■ **Figure 14** Illustration for the proof of Lemma 18.

5 Identifying the Voronoi topologies by exhaustive search

In this section, we present an exhaustive search algorithm to classify the Voronoi diagram of four lines, assuming no full twists. To this end, we use the notion of a *configuration* as an abstraction for a projected bisector and the two relevant trisectors it contains.

We call a planar curve with four non-intersecting components *trisector-like*, if it satisfies the properties of the projected trisector of Lemma 4, in terms of the asymptotes and the middle trisector branch. Each trisector-like curve partitions the plane into faces, which we label as NVD or FVD according to Lemma 4, item 3. If a trisector-like curve is indeed the projected trisector of a set of three lines L , its faces are projections of $NVD(L)$ and $FVD(L)$.

We define a *configuration* on the plane as the overlay of two trisector-like curves. A configuration partitions the plane into faces, which we label as NVD, FVD, or VD_2 . The faces labeled as NVD (resp. FVD) are the common intersections of the respectively labeled faces of the two trisector-like curves; any other face is labeled VD_2 . A configuration is called *realizable* if there exist four lines L that define a bisector and two related trisectors whose projection has the same structure as the configuration. If a configuration is realizable, then the projected faces of $NVD(L)$ (resp. $FVD(L)$ and $VD_2(L)$) on that bisector correspond exactly to the configuration faces labeled as NVD (resp. FVD and VD_2). For example, the configuration in Fig. 15 right is realizable by the projected bisector and trisectors on the left.

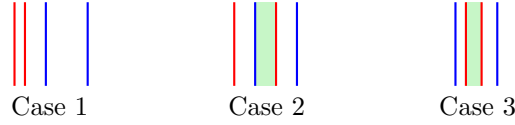


■ **Figure 15** Left: a real projected bisector with two projected trisectors on it. Right: a configuration. Green faces are NVD faces, orange faces are FVD faces, and white faces are VD_2 faces.

5.1 Properties of configurations

We give necessary conditions that restrict how trisectors and their asymptotes interact. These conditions rule out many unrealizable configurations. By Lemma 9, the map $\Gamma(NVD(L))$ has 12 vertices that indicate the unbounded Voronoi edges.

- **Lemma 19.** *Given four lines L in general position, one of the following holds:*
1. *one trisector induces 6 vertices in $\Gamma(\text{NVD}(L))$ and each other trisector induces 2;*
 2. *one trisector induces 0 vertices in $\Gamma(\text{NVD}(L))$ and each other trisector induces 4.*



■ **Figure 16** Three cases for the unbounded parts of two vertical asymptotes. The unbounded NVD face (when present) is shown in green. In Case 1, there is none; in Cases 2 and 3, there is one. Consequently, in Case 1, the red and blue trisectors induce 0 vertices to $\Gamma(\text{NVD}(L))$, while in Cases 2 and 3, they induce 4 vertices.

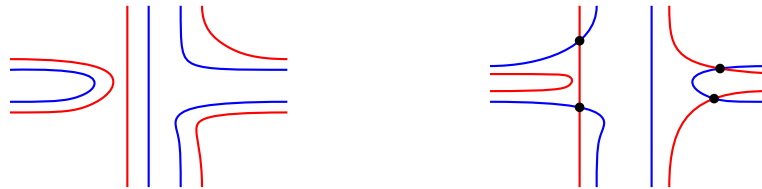
Proof. Consider $\Gamma(\text{NVD}(L))$. It has 12 vertices which correspond to the unbounded edges of $\text{NVD}(L)$. Fix one projected bisector with the two projected trisectors it contains. Each projected trisector has two vertical asymptotes. Up to symmetry, there are three cases, shown in Fig. 16. By Lemma 4, any unbounded NVD face lies between the two red asymptotes and the two blue asymptotes. Horizontal asymptotes behave analogously. Hence, on one bisector, the two trisectors together contribute 0, 4, or 8 vertices to $\Gamma(\text{NVD}(L))$. Let n_1, n_2, n_3, n_4 be the number of vertices of $\Gamma(\text{NVD}(L))$ that are induced by the four trisectors. Then $\sum_{i=1}^4 n_i = 12$, and $n_i + n_j \in \{0, 4, 8\}$, for any $i \neq j$. Up to permutation, the only solutions are $(0, 4, 4, 4)$ and $(2, 2, 2, 6)$. This completes the proof. ◀

A bisector is called an (i, j) -bisector if the two trisectors it contains induce i and j vertices in $\Gamma(\text{NVD}(L))$. As a corollary of Lemma 19, we obtain the following classification of bisectors.

- **Corollary 20.** *Given four lines L in general position, one of the following holds:*
1. *there are three $(2, 2)$ -bisectors and three $(2, 6)$ -bisectors (with respect to $\Gamma(\text{NVD}(L))$);*
 2. *there are three $(0, 4)$ -bisectors and three $(4, 4)$ -bisectors (with respect to $\Gamma(\text{NVD}(L))$).*

► **Lemma 21.** *Consider a bisector with two projected trisectors T_i, T_j . Let x_i^-, x_i^+ ($x_i^- < x_i^+$) (resp. y_i^-, y_i^+) be the two vertical (resp. horizontal) asymptotes of T_i ; analogously for T_j . It is impossible that simultaneously $x_i^- < x_j^- < x_j^+ < x_i^+$ and $y_j^- < y_i^- < y_i^+ < y_j^+$.*

Proof. By the formula in the proof of Lemma 5, the vertical asymptotes of a trisector T_i are $x_i^\pm = \frac{e_i A}{a} \pm \sqrt{A \Delta_i}$, where $A = 1 + a^2$ and $\Delta_i = d_i^2 + e_i^2 + 1$. Thus, $x_i^- < x_j^- < x_j^+ < x_i^+$ is equivalent to $\sqrt{\Delta_j} - \sqrt{\Delta_i} < \frac{(e_i - e_j)\sqrt{A}}{a} < \sqrt{\Delta_i} - \sqrt{\Delta_j}$. Similarly, the horizontal asymptotes of a trisector T_i are $y_i^\pm = \frac{d_i A \pm \sqrt{A \Delta_i}}{a}$. Therefore, $y_j^- < y_i^- < y_i^+ < y_j^+$ is equivalent to $\sqrt{\Delta_i} - \sqrt{\Delta_j} < (d_i - d_j)\sqrt{A} < \sqrt{\Delta_j} - \sqrt{\Delta_i}$. It is not hard to verify that the two relations contradict each other. This completes the proof. ◀

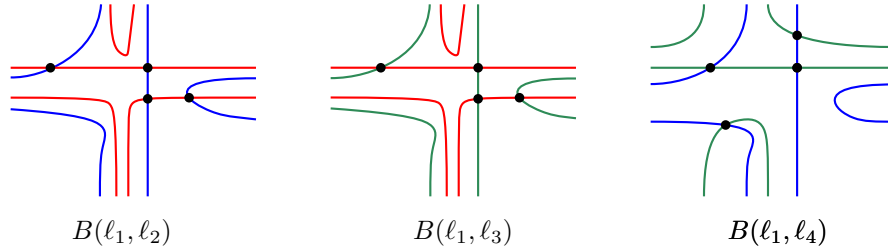


■ **Figure 17** Left: a $(0, 8)$ -bisector, impossible by Corollary 20. Right: impossible by Lemma 21.

We apply Corollary 20 and Lemma 21 to filter out unrealizable configurations such as those illustrated in Fig. 17.

We say that two related trisectors (on a bisector) are *parallel* (denoted “ $\cdot \parallel \cdot$ ”), if they are both x -monotone or both y -monotone; otherwise, they are not parallel (“ $\cdot \not\parallel \cdot$ ”). Parallelism of trisectors is transitive. The following is used as a filter in Section 5.2.

► **Lemma 22.** *For any three pairwise related trisectors T_i, T_j, T_k , if $T_i \parallel T_j$ and $T_j \parallel T_k$, then $T_i \parallel T_k$; if $T_i \not\parallel T_j$ and $T_j \not\parallel T_k$, then $T_i \parallel T_k$; see Fig. 18.*



■ **Figure 18** Three bisectors and trisectors; $T(\ell_1, \ell_2, \ell_3)$ is red, $T(\ell_1, \ell_2, \ell_4)$ is blue, $T(\ell_1, \ell_3, \ell_4)$ is green. They are not realizable by Lemma 22.

Proof. WLOG, we may assume that T_i, T_j, T_k are $T(\ell_1, \ell_2, \ell_3)$, $T(\ell_1, \ell_2, \ell_4)$, and $T(\ell_1, \ell_3, \ell_4)$ respectively. Consider $\Gamma(\text{FVD}(L))$ and the following function that projects away from the line ℓ_1 : for $x \in T$, let y_x be the nearest point on ℓ_1 to x , let $\pi : T \rightarrow \Gamma$ be the projection such that $\pi(x) = \overrightarrow{y_x x} \cap \Gamma$. Consider $\pi(M)$, where M is the middle branch of T . Since M has only one asymptote (Lemma 4), $M \cap \Gamma$ are two points that are antipodal in the limit when $\Gamma \rightarrow \infty$. To be precise, let $\{x_1, x_2\} = M \cap \Gamma$, then $\lim_{\Gamma \rightarrow \infty} x_1 + x_2 = 0$. For the rest of the proof, all statements hold under the assumption that $\Gamma \rightarrow \infty$.

The intersections of $\pi(T(\ell_1, \ell_2, \ell_3))$ and $\pi(T(\ell_1, \ell_2, \ell_4))$ are in one-to-one correspondence with the intersections of $T(\ell_1, \ell_2, \ell_3)$ and $T(\ell_1, \ell_2, \ell_4)$. Two middle trisector branches are parallel if and only if they intersect an even number of times (including 0), equivalently, their projections intersect an even number of times. It is not hard to verify that this property is transitive. ◀

Next, we consider *6-tuples of configurations*, where each configuration corresponds to one bisector associated with four lines. A configuration tuple is realizable if and only if there exists a set of four lines that realizes every configuration in the tuple. In a realizable 6-tuple, each trisector-like curve (12 in total) represents a trisector $T(\ell_i, \ell_j, \ell_k)$ whose representation must be consistent with all the elementary properties listed in Section 2 and Lemma 4 (by viewing a configuration as a bisector and a trisector-like curve as a trisector). Note that there are exactly three trisector-like curves that represent $T(\ell_1, \ell_2, \ell_3)$, and they lie on the configurations of $B(\ell_1, \ell_2)$, $B(\ell_1, \ell_3)$, and $B(\ell_2, \ell_3)$.

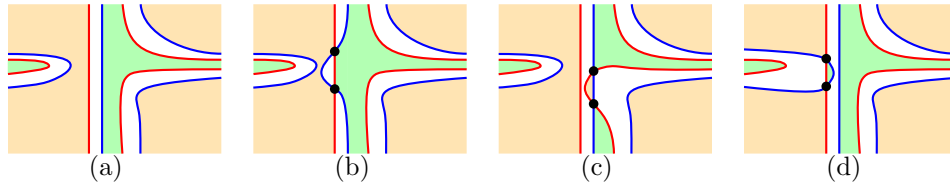
5.2 A search algorithm, proving Theorems 1 and 2

To classify the topology of the Voronoi diagram of four lines without full twists, we use the following exhaustive search algorithm.

Phase 1: Generate configurations. We generate all configurations with at most 8 vertices, excluding those that lead to full twists. Phase 1 works in two steps.

In Step 1, we generate simple configurations that have no twists. By Lemma 4, such a configuration is uniquely determined by the asymptotes and the choice of the middle branches. We construct the simple configurations by enumerating all asymptote arrangements and all choices of middle branches of the two trisector-like curves. We label the faces of each configuration as described above.

In Step 2, we add twists to simple configurations, as many as possible, provided that the number of resulting vertices is at most 8. To add a twist, we select two configuration edges that bound an existing face, fix their endpoints, and intersect their interior twice more. To avoid creating full twists, we only consider edge pairs incident to a face with label VD_2 (see Fig. 19 (a)-(b)). This is sufficient because intersecting any other pair of edges produces a full twist, as shown in the proof of Theorem 1.



■ **Figure 19** (a) A simple configuration. Faces labeled NVD (resp. FVD) are shown in green (resp. orange). (b) Add a twist by intersecting two edges bounding a VD_2 face (in white). (c), (d) Add a twist by intersecting two edges bounding an NVD or FVD face; both lead to a full twist.

Phase 2: Filter out configurations. We filter out any configurations of Phase 1 that are not realizable by applying filters derived from Corollary 20 and Lemma 21.

Phase 3: Filter out unrealizable configuration tuples. We generate all possible configuration 6-tuples from the configurations that remain at the end of Phase 2. We filter out unrealizable tuples by applying filters derived from the elementary properties of Section 2, Corollary 20, Lemma 22, and Theorem 10, and obtain the set \mathcal{P} of configuration tuples that survive these filters. Since the search space is large, we implement the filters in a program [22], which outputs 15 remaining configuration tuples at the end of Phase 3.

Each surviving configuration tuple in \mathcal{P} can be realized by a set of four lines. We give an example for each one in Appendix A. Each configuration tuple in \mathcal{P} corresponds to a unique Voronoi diagram topology as shown in the proof of Theorem 1. Then, straightforward inspection of the tuples and their topologies reveals the following properties.

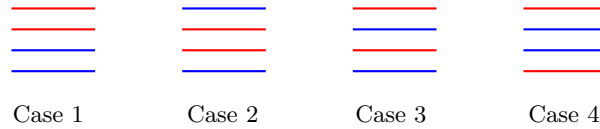
- **Observation 23.** *Assuming no full twists, the following hold for $NVD(L)$ and $FVD(L)$.*
1. *Topologies with 0 or 2 vertices have no partial twists in their trisector system.*
 2. *Topologies with 4 or more vertices have at least one partial twist.*
 3. *No topology has 8 vertices; hence 8 Voronoi vertices require the presence of full twists.*
 4. *The 2D faces of both $NVD(L)$ and $FVD(L)$ are all unbounded.*
 5. *Each distinct FVD topology has a distinct map of unbounded features $\Gamma(FVD(L))$.*
 6. *There are only two distinct maps $\Gamma(NVD(L))$, each corresponding to a case of Lemma 19.*
 7. *A partial twist involves at least two middle trisector branches, each incident to exactly one vertex of the partial twist.*
 8. *The 1-skeleton of $NVD(L)$ has a single connected component that contains all vertices. This does not hold for $FVD(L)$.*
 9. *The edges of $FVD(L)$ are unbounded except those incident to both vertices of a partial twist.*

Before proving Theorem 1, we show that Step 1 in Phase 1 works correctly.

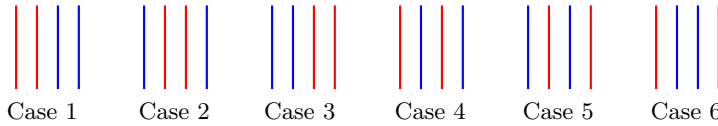
► **Lemma 24.** *There is a way to enumerate the set of all configurations with no twists, i.e., the simple configurations, such as the one in Step 1 in Phase 1 of the exhaustive search algorithm.*

Proof. For simplicity, let the two trisector-like curves in a configuration be red and blue respectively. It is easy to see that a configuration with no twists is uniquely determined by (1) the arrangement of the red and blue asymptotes (both horizontal and vertical) and (2) the choices of the red and blue middle branches. WLOG, we fix the blue trisector-like curve to have the shape illustrated in Fig. 1, i.e., the asymptote of its middle branch is the right vertical asymptote and its shape is vertically symmetric.

The horizontal (resp. vertical) asymptotes of the red trisector-like curve have four (resp. six) different possible arrangements with respect to the blue asymptotes, shown in Figs. 20 and 21 respectively.



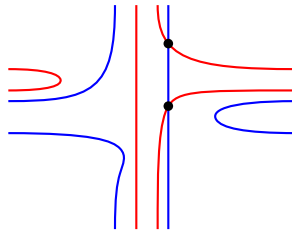
■ **Figure 20** Four horizontal asymptote arrangements.



■ **Figure 21** Six vertical asymptote arrangements.

Next, we determine the asymptote of the middle branch of the red trisector-like curve, which has four choices: upper horizontal, lower horizontal, left vertical, and right vertical. This gives a systematic way to enumerate all simple configurations, which is adopted in Step 1. ◀

As an example of the enumeration process above, if we choose horizontal asymptote arrangement (Case 1), vertical asymptote arrangement (Case 2), and left vertical asymptotes for the red middle branch, we obtain the simple configuration shown in Fig. 22. Further, the proof shows that the number of simple configurations is upper bounded by $96 (= 4 \times 6 \times 4)$. In fact, the number is smaller as some of them are symmetric to each other by rotation, mirror symmetry, or swap of colors.



■ **Figure 22** A simple configuration with two vertices.

Next, we explain how to construct the Voronoi diagram from a configuration tuple output at the end of Phase 3. For this purpose, we assume that the edges and vertices in each configuration of the tuple are labeled in a way consistent with the filtering conditions of Phase 3. See Appendix A for the 15 labeled configuration tuples.

► **Lemma 25.** *Given a labeled configuration tuple, there is at most one matching topology for the nearest Voronoi diagram of four lines. Similarly for the farthest counterpart.*

Proof. We show how to reconstruct the diagram uniquely (up to mirror symmetry) given the label information of the configuration tuple. First, we may assume that all edges are oriented. If an edge is incident to at least one vertex, then the orientation is given by the label of the vertex. Otherwise, the edge is a whole trisector branch, in which case locally around the edge, the diagram is the Voronoi diagram of three lines, which has a fixed structure [12]. Hence, an edge in a labeled configuration tuple has a fixed orientation.

Start with an arbitrary edge and the three faces incident to it. Glue the faces along the edge while respecting its orientation. This determines a unique local structure up to mirror symmetry (see the proof of Lemma 14 and Fig. 4). The local Voronoi regions around the faces are fixed. We then build the diagram incrementally, adding one face in each step.

Assume that we have a partially constructed diagram D . Let f be a new face that shares an edge e with D . Then there is a unique way to attach f along e that respects the orientation of e (see the proof of Lemma 14 and Fig. 4).

By [5] Theorem 3.7, the farthest Voronoi diagrams of lines have connected 2-skeletons. The nearest counterpart also has connected 2-skeletons, which can be easily shown by induction where the base case of three lines follows from [12]. Therefore, there is a sequence of faces that incrementally build the whole diagram. Consequently, the resulting diagram is unique up to mirror symmetry. ◀

Proof of Theorem 1. Phase 1, Step 1 generates all the simple configurations that have no twists, by Lemma 24. Next, we argue that Step 2 correctly considers only the edges incident to faces labeled VD_2 in order to generate all possible partial twists.

Consider two arbitrary edges e_1 and e_2 in a simple configuration from Step 1. If e_1 and e_2 are incident to a common face labeled NVD (resp. FVD), intersecting them twice creates a bounded face with two vertices labeled FVD (resp. NVD), see Fig. 19 (c) and (d) respectively. By Lemma 17, such a face yields a full twist. Assume now that e_1 and e_2 are not incident to a common configuration face. To intersect them, there must be at least one intermediate edge e_3 such that we first intersect e_1 and e_3 twice, after which e_1 and e_2 may become adjacent, and then we can intersect e_1, e_2 twice. This is captured by Fig. 12. By Lemma 18, the twist between e_1 and e_2 is a full twist. The case when there is more than one intermediate edge between e_1 and e_2 can be handled analogously. Hence, Step 2 correctly considers edges that are only incident to faces labeled as VD_2 , and this is enough to generate all the relevant configurations.

Phases 2 and 3 use filters derived from the necessary conditions on the diagrams that have already been proved. Thus, the output set \mathcal{P} of Phase 3 contains every configuration tuple that may be realizable. Examples in Appendix A verify that the configuration tuples in \mathcal{P} are realizable.

Each configuration tuple fixes the vertices, edges, and faces of all six configurations. By Lemma 25, these features can be glued uniquely to form the Voronoi diagram. Thus, there are 15 topologies for each of $NVD(L)$ and $FVD(L)$, which are in one-to-one correspondence with the configuration 6-tuples, and thus they are in one-to-one correspondence to each other. The correspondence naturally extends to $VD_2(L)$. The remaining assertions of the theorem

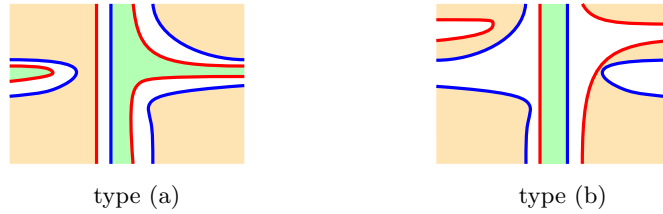
follow from inspecting the 15 configuration tuples listed in Appendix A. This completes the proof. ◀

As already mentioned, all configuration tuples that survive Phase 3 are realizable. This is crucial for the proof of Theorem 2, and further implies that the necessary conditions of the filters are also sufficient.

Proof of Theorem 2. Consider four lines and their four trisectors. If there are no full twists in the trisector system, then the Voronoi diagram falls into one of the 15 topologies of Theorem 1. Assume that there are some full twists; by Lemma 13 they cannot be nested. Any full twist can be removed locally by the reverse local modification described in Section 4.1. Furthermore, if a configuration tuple satisfies the filters of the exhaustive search algorithm, then the configuration tuple derived after the removal of a full twist also does. Hence, the resulting configuration tuple, after removing all full twists, is one of the 15 configuration tuples in \mathcal{P} , all of which are realizable. This completes the proof. ◀

6 Examples and concluding remarks

Example 1: Voronoi diagram of four lines with 0 vertices. Assuming that there are 0 vertices, there are only two configurations (type (a) and type (b)) that satisfy Corollary 20 and Lemma 21; see Fig. 23. Only one 6-tuple of configurations satisfies Corollary 20: three configurations of type (a) and three of type (b).

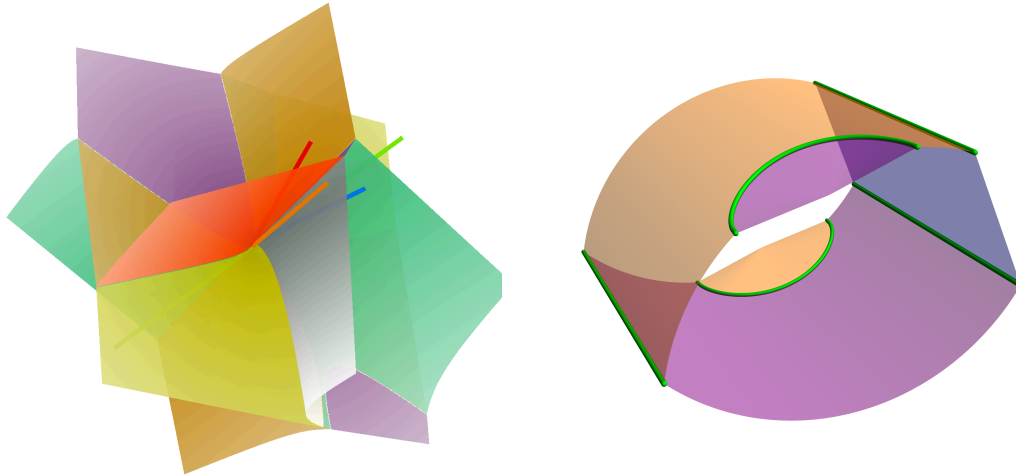


■ **Figure 23** Two configurations with 0 vertices. Faces with label NVD, FVD, and VD_2 are in green, orange, and white, respectively. Type (a) gives a $(2,6)$ -bisector and type (b) gives a $(2,2)$ -bisector.

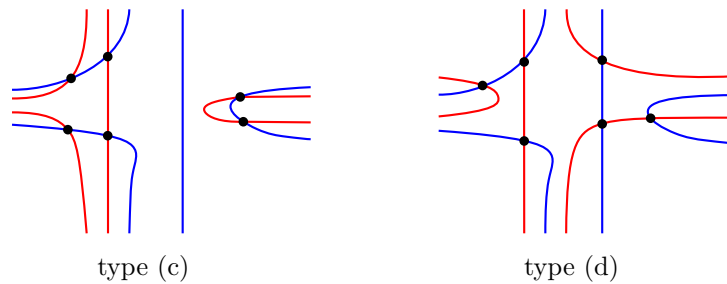
An NVD example is shown in Fig. 24 left. Of the four Voronoi regions, one is an unbounded triangular prism with three side faces (the region of the orange line in Fig. 24 left); the other three have identical structure, which is schematically illustrated in Fig. 24 right. The farthest Voronoi diagram is depicted schematically in Fig. 26 left.

Example 2: Voronoi diagram of four lines with 6 vertices. We show an example where the 6-tuple of configurations is symmetric: it consists of three configurations of type (c) and three of type (d), shown in Fig. 25. The FVD is shown schematically in Fig. 26 right.

Our classification results yield an algebraically simple method to compute the structure of the Voronoi diagram of four lines. We start by computing the Gaussian map of $FVD(L)$ [5], which is simple algebraically. We then extract $\Gamma(FVD(L))$ by a minor adjustment (concerning the so-called vertices of anomaly of [5]). From $\Gamma(FVD(L))$, we can directly identify the matching base topologies of $NVD(L)$ and $FVD(L)$. Next, we decide if full twists exist by comparing the number of vertices in the base topology with the number of projected trisector intersections. The latter equals the number of real roots of a degree 8 univariate polynomial, which we compute via Sturm's theorem. If equal, there are no full twists, and the base topology provides the answer; otherwise, we need to locate the full twists. To this end, we



■ **Figure 24** Left: $\text{NVD}(L)$ with 0 vertices, faces in the same color are from the same bisector. Right: schematic illustration of a Voronoi region of $\text{NVD}(L)$. Compare this with a region in the Voronoi diagram of three lines shown in Fig. 8 middle.



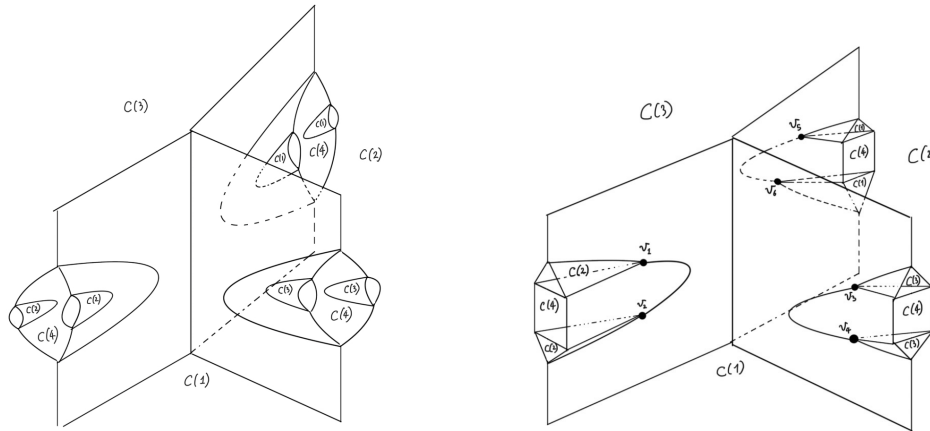
■ **Figure 25** Two configuration types involved in Example 2.

derive the real configurations of each bisector (by applying the separation of four branches of a trisector given in [12] to obtain (1) the corresponding simple configurations as in Phase 1, and (2) the number of intersections between all pairs of trisector branches). We compare with the configurations of the base topology, revealing the vertices of full twists, and add them to the base topology via the local modification. All operations can be done in low algebraic degrees, the most expensive being the location of full twists (whose degree is in the range of 8).

In conclusion, we have obtained a complete characterization of Voronoi diagrams of four lines in general position in \mathbb{R}^3 . This offers a concrete foundation for future research on the Voronoi diagrams of n lines.

References

- 1 Pankaj K Agarwal, Boris Aronov, and Micha Sharir. Computing envelopes in four dimensions with applications. In *Proceedings of the tenth annual symposium on Computational geometry*, pages 348–358, 1994.
- 2 Boris Aronov. A lower bound on Voronoi diagram complexity. *Information Processing Letters*, 83(4):183–185, 2002.



■ **Figure 26** Left: schematic of the $FVD(L)$ with 0 vertices. Right: schematic of the $FVD(L)$ with 6 vertices of Example 2. Each label $C(i)$ denotes a cell in the farthest region of ℓ_i .

- 3 Franz Aurenhammer, Bert Jüttler, and Günter Paulini. Voronoi diagrams for parallel halflines and line segments in space. In *28th International Symposium on Algorithms and Computation (ISAAC 2017)*. Schloss Dagstuhl-Leibniz-Zentrum fuer Informatik, 2017.
- 4 Franz Aurenhammer, Evanthia Papadopoulou, and Martin Suderland. Piecewise-linear farthest-site Voronoi diagrams. In *32nd International Symposium on Algorithms and Computation (ISAAC 2021)*, pages 327–345. Schloss Dagstuhl-Leibniz-Zentrum für Informatik, 2021.
- 5 Gill Barequet, Evanthia Papadopoulou, and Martin Suderland. Unbounded regions of high-order Voronoi diagrams of lines and line segments in higher dimensions. *Discrete & Computational Geometry*, pages 1–29, 2023.
- 6 Jean-Daniel Boissonnat, Micha Sharir, Boaz Tagansky, and Mariette Yvinec. Voronoi diagrams in higher dimensions under certain polyhedral distance functions. In *Proceedings of the eleventh annual symposium on Computational geometry*, pages 79–88, 1995.
- 7 Bernard Chazelle. An optimal convex hull algorithm and new results on cuttings (extended abstract). In *32nd Annual Symposium on Foundations of Computer Science, San Juan, Puerto Rico*, pages 29–38. IEEE Computer Society, 1991.
- 8 L Paul Chew, Klara Kedem, Micha Sharir, Boaz Tagansky, and Emo Welzl. Voronoi diagrams of lines in 3-space under polyhedral convex distance functions. *Journal of Algorithms*, 29(2):238–255, 1998.
- 9 Tamal K Dey and Wulue Zhao. Approximate medial axis as a Voronoi subcomplex. In *Proceedings of the seventh ACM symposium on Solid modeling and applications*, pages 356–366, 2002.
- 10 Herbert Edelsbrunner and Raimund Seidel. Voronoi diagrams and arrangements. *Discrete & Computational Geometry*, 1:25–44, 1986.
- 11 Michal Etzion and Ari Rappoport. Computing the Voronoi diagram of a 3-d polyhedron by separate computation of its symbolic and geometric parts. In *Proceedings of the fifth ACM symposium on Solid modeling and applications*, pages 167–178, 1999.
- 12 Hazel Everett, Daniel Lazard, Sylvain Lazard, and Mohab Safey El Din. The Voronoi diagram of three lines. *Discrete & Computational Geometry*, 42(1):94–130, 2009.
- 13 Marc Glisse. Lower bound on the Voronoi diagram of lines in \mathbb{R}^d , 2021. URL: <https://arxiv.org/abs/2103.17251>, arXiv:2103.17251.
- 14 Michael Hemmer, Ophir Setter, and Dan Halperin. Constructing the exact Voronoi diagram of arbitrary lines in three-dimensional space: with fast point-location. In *European Symposium on Algorithms*, pages 398–409. Springer, 2010.

- 15 Christian Icking and Lihong Ha. A tight bound for the complexity of Voronoi diagrams under polyhedral convex distance functions in 3d. In *Proceedings of the thirty-third annual ACM symposium on Theory of computing*, pages 316–321, 2001.
- 16 Victor Klee. On the complexity of d-dimensional Voronoi diagrams. *Archiv der Mathematik*, 34(1):75–80, 1980.
- 17 Vladlen Koltun and Micha Sharir. Polyhedral Voronoi diagrams of polyhedra in three dimensions. In *Proceedings of the eighteenth annual symposium on Computational geometry*, pages 227–236, 2002.
- 18 Vladlen Koltun and Micha Sharir. Three dimensional Euclidean Voronoi diagrams of lines with a fixed number of orientations. In *Proceedings of the eighteenth annual symposium on Computational geometry*, pages 217–226, 2002.
- 19 Joseph S. B. Mitchell and Joseph O’Rourke. Computational geometry column 42. *International Journal of Computational Geometry & Applications*, 11(5):573–582, 2001.
- 20 Raimund Seidel. On the number of faces in higher-dimensional Voronoi diagrams. In *Proceedings of the third annual symposium on Computational geometry*, pages 181–185, 1987.
- 21 Micha Sharir. Almost tight upper bounds for lower envelopes in higher dimensions. *Discrete & Computational Geometry*, 12:327–345, 1994.
- 22 Zeyu Wang. Search engine for the Voronoi diagram of four lines in \mathbb{R}^3 , March 2026. URL: <https://github.com/ze-yu-wang/Voronoi-diagram-of-4-lines-program.git>.

Appendix

A Topologies of the Voronoi diagram of four lines without full twists

We describe the 15 topologies of the Voronoi diagram of four lines without full twists. For each topology, we list the following:

- the configuration tuple of the six projected bisectors and their trisectors;
- a set L of four lines realizing the configuration tuple;
- the map of unbounded features $\Gamma(\text{FVD}(L))$.

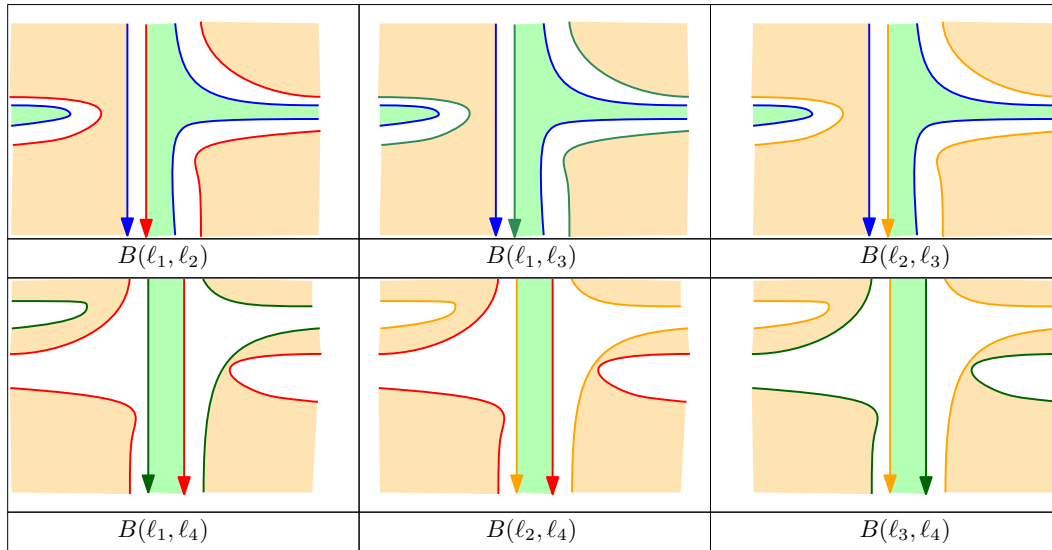
Note that we do not show the 3D Voronoi diagram figures for the real examples. The real diagrams are curved and complex, see Fig. 24 left for the simplest example with 0 vertices. So we feel that such figures do not provide much additional information to the diagrams.

To illustrate that the examples we provide indeed realize the configuration tuple, we also show the real projected bisectors of these lines, each containing two projected trisectors. By comparing the real projected bisectors (with their trisectors) and the configurations, we finish the verification of the examples.

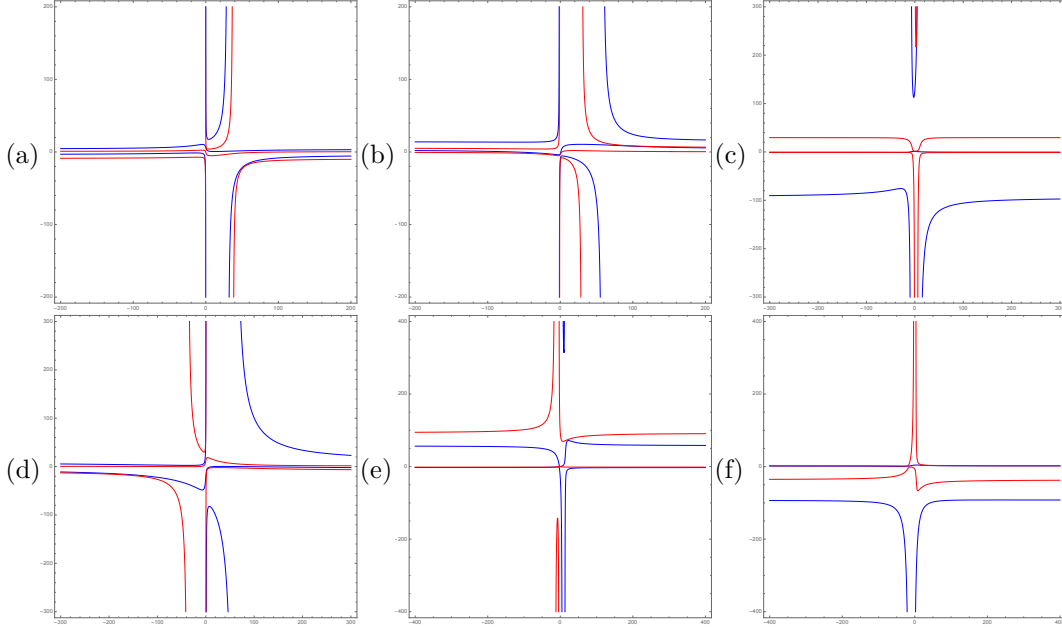
For practical reasons, we may not show all the trisector branches or vertices on some real projected bisector examples. For example, a vertex might not be shown because including it would cause the figure to zoom out much further and the result would be much harder to read. However, we make sure that all missing features can be recovered easily manually, following the basic properties of a projected trisector in Lemma 4.

A.1 Topology I: 0 vertices

The configuration tuple that induces topology I is shown in Fig. 27. A set of lines that realizes this tuple, hence this topology, has the following parameters: $(a, b_3, c_3, d_3, e_3, b_4, c_4, d_4, e_4) = (-9, 2, -2, 1, -3, -1, 1, -1, -5)$. Fig. 28 shows the six projected bisectors of these four lines, which match the configurations shown in Fig. 27. The $\Gamma(\text{FVD}(L))$ is shown in Fig. 29.



■ **Figure 27** Combination that forms topology I.



■ **Figure 28** Six projected bisectors when the four lines have the following parameters: $(a, b_3, c_3, d_3, e_3, b_4, c_4, d_4, e_4) = (-9, 2, -2, 1, -3, -1, 1, -1, -5)$. They match the configurations shown in Fig. 27 and form topology I.

A.2 Topology II: 2 vertices

The configuration tuple that induces topology II is shown in Fig. 30. A set of lines that realizes this tuple, hence this topology, has the following parameters: $(a, b_3, c_3, d_3, e_3, b_4, c_4, d_4, e_4) = (-3, -16, -12, -3, 9, -10, 1, 9, -11)$. Fig. 31 shows the six projected bisectors of these four lines, which match the configurations shown in Fig. 30. The $\Gamma(\text{FVD}(L))$ is shown in Fig. 32.

A.3 Topology III: 2 vertices

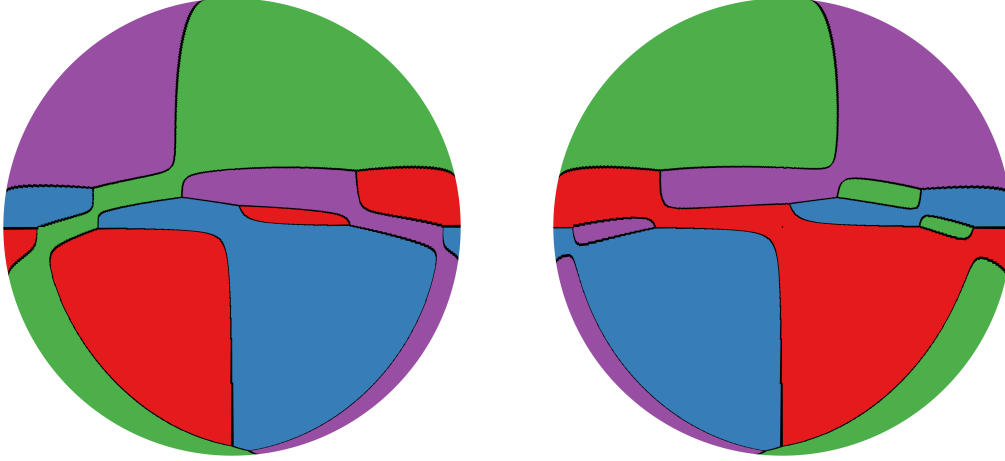
The configuration tuple that induces topology III is shown in Fig. 33. A set of lines that realizes this tuple, hence this topology, has the following parameters: $(a, b_3, c_3, d_3, e_3, b_4, c_4, d_4, e_4) = (-4, 5, 10, 3, 4, 5, 6, -1, 1)$. Fig. 34 shows the six projected bisectors of these four lines, which match the configurations shown in Fig. 33. The $\Gamma(\text{FVD}(L))$ is shown in Fig. 35.

A.4 Topology IV: 2 vertices

The configuration tuple that induces topology IV is shown in Fig. 36. A set of lines that realizes this tuple, hence this topology, has the following parameters: $(a, b_3, c_3, d_3, e_3, b_4, c_4, d_4, e_4) = (4, -9, -8, -6, -1, 10, -1, 0, -1)$. Fig. 37 shows the six projected bisectors of these four lines, which match the configurations shown in Fig. 36. The $\Gamma(\text{FVD}(L))$ is shown in Fig. 38.

A.5 Topology V: 4 vertices

The configuration tuple that induces topology V is shown in Fig. 39. A set of lines that realizes this tuple, hence this topology, has the following parameters: $(a, b_3, c_3, d_3, e_3, b_4, c_4, d_4, e_4) = (1, -19, 11, 7, 16, -11, 1, -12, 6)$. Fig. 40 shows the six projected bisectors of these four lines, which match the configurations shown in Fig. 39. The $\Gamma(\text{FVD}(L))$ is shown in Fig. 41.



■ **Figure 29** Top and bottom view of $\Gamma(\text{FVD}(L))$ of topology I.

A.6 Topology VI: 4 vertices

The configuration tuple that induces topology VI is shown in Fig. 42. A set of lines that realizes this tuple, hence this topology, has the following parameters: $(a, b_3, c_3, d_3, e_3, b_4, c_4, d_4, e_4) = (16, -10, 3, 0, -1, 5, 1, 2, 5)$. Fig. 43 shows the six projected bisectors of these four lines, which match the configurations shown in Fig. 42. The $\Gamma(\text{FVD}(L))$ is shown in Fig. 44.

A.7 Topology VII: 4 vertices

The configuration tuple that induces topology VII is shown in Fig. 45. A set of lines that realizes this tuple, hence this topology, has the following parameters: $(a, b_3, c_3, d_3, e_3, b_4, c_4, d_4, e_4) = (4, 7, 9, 1, 10, -3, -10, 6, -8)$. Fig. 46 shows the six projected bisectors of these four lines, which match the configurations shown in Fig. 45. The $\Gamma(\text{FVD}(L))$ is shown in Fig. 47.

A.8 Topology VIII: 4 vertices

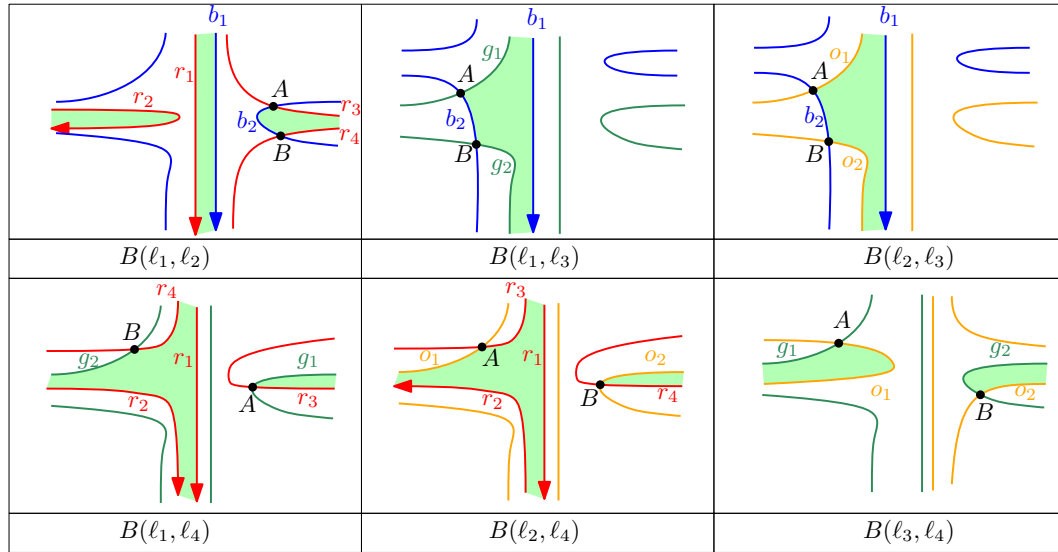
The configuration tuple that induces topology VIII is shown in Fig. 48. A set of lines that realizes this tuple, hence this topology, has the following parameters: $(a, b_3, c_3, d_3, e_3, b_4, c_4, d_4, e_4) = (2, -19, -4, -13, 20, 14, -18, -3, 9)$. Fig. 49 shows the six projected bisectors of these four lines, which match the configurations shown in Fig. 48. The $\Gamma(\text{FVD}(L))$ is shown in Fig. 50.

A.9 Topology IX: 4 vertices

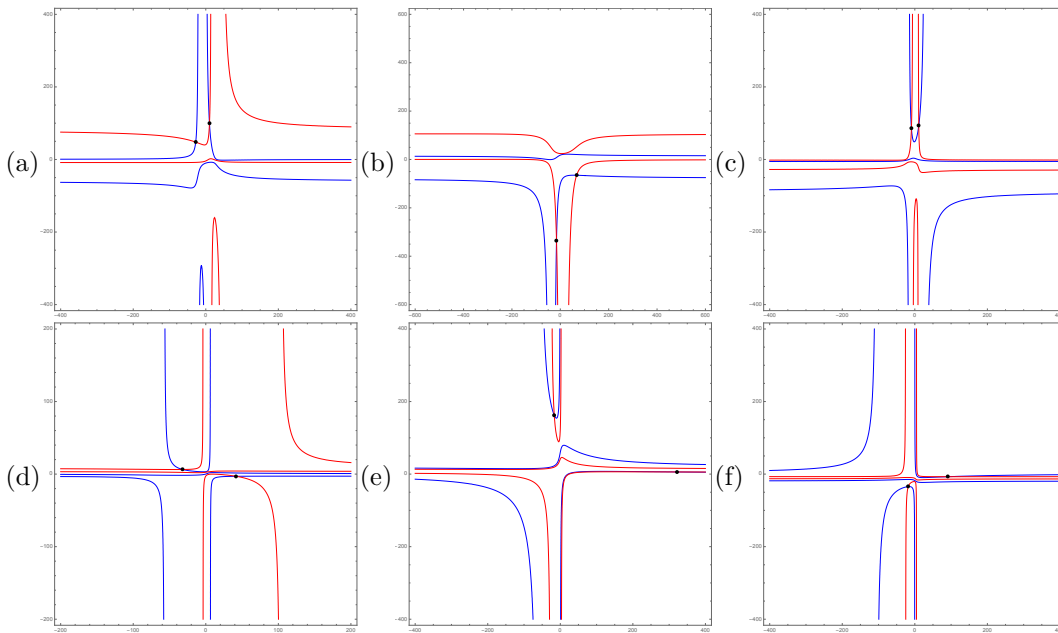
The configuration tuple that induces topology IX is shown in Fig. 51. A set of lines that realizes this tuple, hence this topology, has the following parameters: $(a, b_3, c_3, d_3, e_3, b_4, c_4, d_4, e_4) = (10, 8, -15, -2, 15, 12, 9, -2, 4)$. Fig. 52 shows the six projected bisectors of these four lines, which match the configurations shown in Fig. 51. The $\Gamma(\text{FVD}(L))$ is shown in Fig. 53.

A.10 Topology X: 6 vertices

The configuration tuple that induces topology X is shown in Fig. 54. A set of lines that realizes this tuple, hence this topology, has the following parameters: $(a, b_3, c_3, d_3, e_3, b_4, c_4, d_4, e_4) = (1, -18, -5, -4, -16, 11, -18, -6, -3)$. Fig. 55 shows the six projected bisectors of these four lines, which match the configurations shown in Fig. 54. The $\Gamma(\text{FVD}(L))$ is shown in Fig. 56.



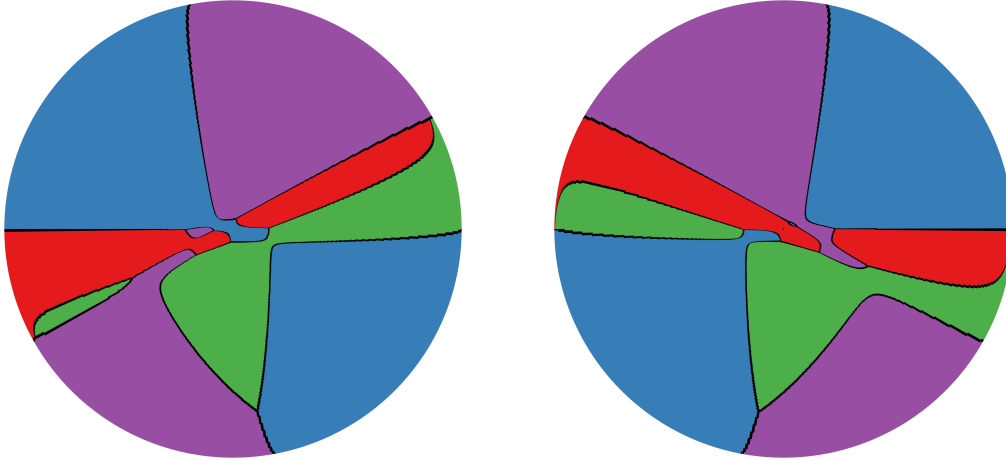
■ **Figure 30** Combination that forms topology II.



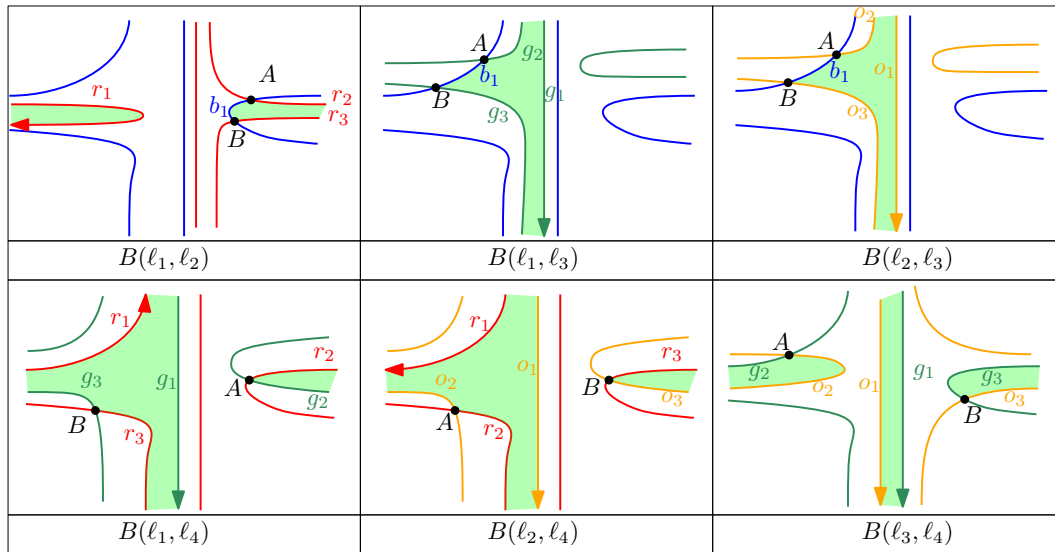
■ **Figure 31** Six projected bisectors when the four lines have the following parameters: $(a, b_3, c_3, d_3, e_3, b_4, c_4, d_4, e_4) = (-3, -16, -12, -3, 9, -10, 1, 9, -11)$. They match the configurations shown in Fig. 30 and form topology II.

A.11 Topology XI: 6 vertices

The configuration tuple that induces topology XI is shown in Fig. 57. A set of lines that realizes this tuple, hence this topology, has the following parameters: $(a, b_3, c_3, d_3, e_3, b_4, c_4, d_4, e_4) = (1, 29, 4, 2, 20, 11, 25, 0, -3)$. Fig. 58 shows the six projected bisectors of these four lines, which match the configurations shown in Fig. 57. The $\Gamma(\text{FVD}(L))$ is shown in Fig. 59.



■ **Figure 32** Top and bottom view of $\Gamma(\text{FVD}(L))$ of topology II.



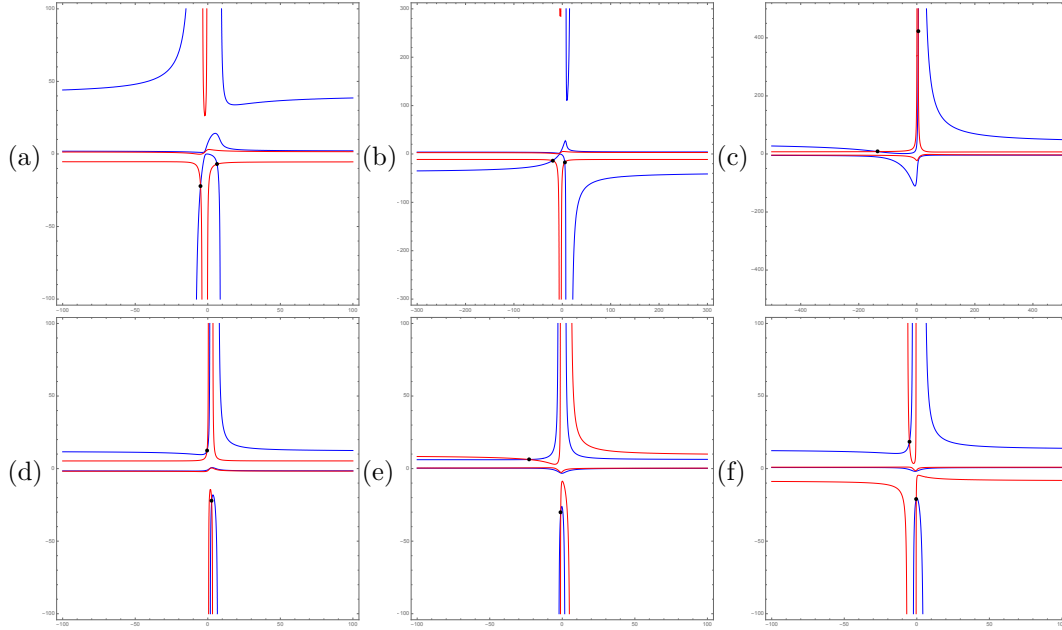
■ **Figure 33** Combination that forms topology III.

A.12 Topology XII: 6 vertices

The configuration tuple that induces topology XII is shown in Fig. 60. A set of lines that realizes this tuple, hence this topology, has the following parameters: $(a, b_3, c_3, d_3, e_3, b_4, c_4, d_4, e_4) = (2, 3, -6, -3, 16, -1, -12, -3, -19)$. Fig. 61 shows the six projected bisectors of these four lines, which match the configurations shown in Fig. 60. The $\Gamma(\text{FVD}(L))$ is shown in Fig. 62.

A.13 Topology XIII: 6 vertices

The configuration tuple that induces topology XIII is shown in Fig. 63. A set of lines that realizes this tuple, hence this topology, has the following parameters: $(a, b_3, c_3, d_3, e_3, b_4, c_4, d_4, e_4) = (5, 7, -10, 0, 2, 16, 7, 0, -16)$. Fig. 64 shows the six projected bisectors of these four lines, which match the configurations shown in Fig. 63. The $\Gamma(\text{FVD}(L))$ is shown in Fig. 65.



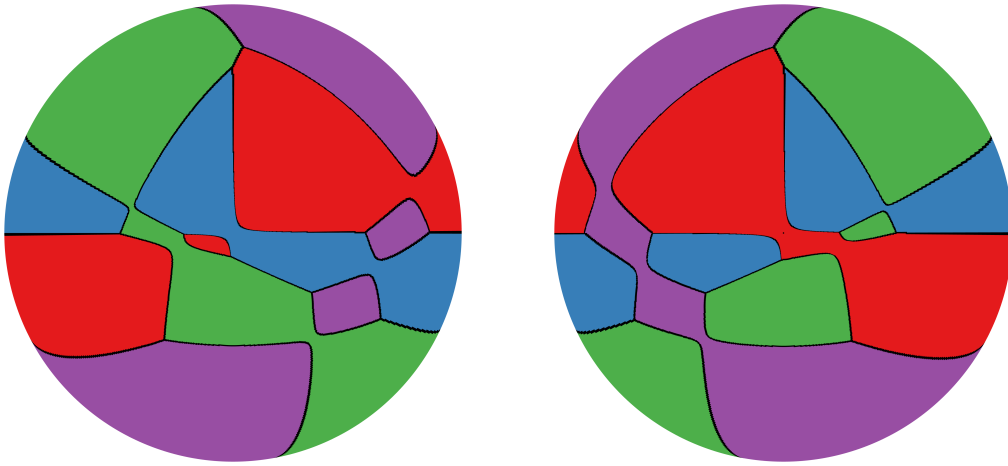
■ **Figure 34** Six projected bisectors when the four lines have the following parameters: $(a, b_3, c_3, d_3, e_3, b_4, c_4, d_4, e_4) = (-4, 5, 10, 3, 4, 5, 6, -1, 1)$. They match the configurations shown in Fig. 33 and form topology III.

A.14 Topology XIV: 6 vertices

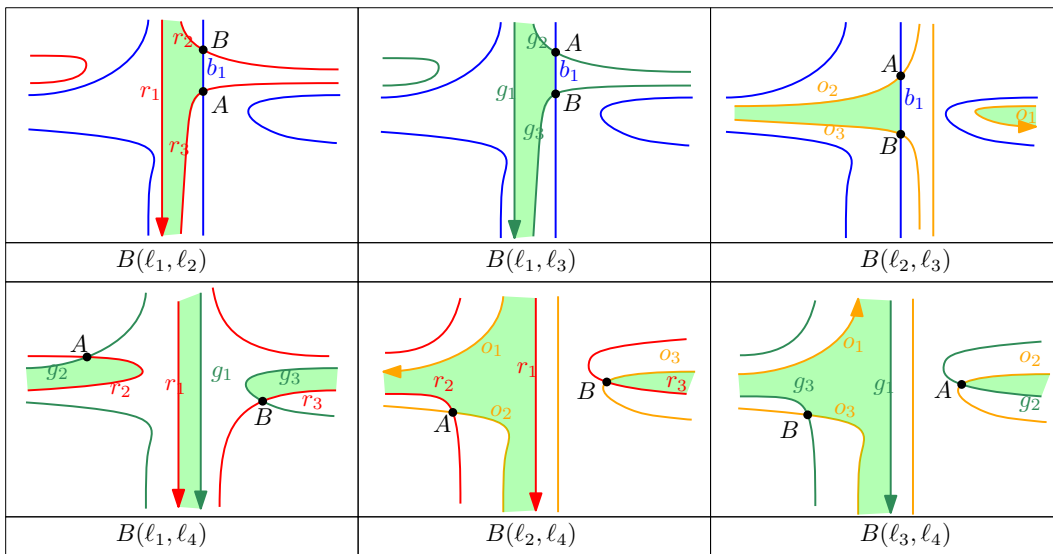
The configuration tuple that induces topology XIV is shown in Fig. 66. A set of lines that realizes this tuple, hence this topology, has the following parameters: $(a, b_3, c_3, d_3, e_3, b_4, c_4, d_4, e_4) = (3, 17, 9, 0, 19, 11, -16, 2, -8)$. Fig. 67 shows the six projected bisectors of these four lines, which match the configurations shown in Fig. 66. The $\Gamma(\text{FVD}(L))$ is shown in Fig. 68.

A.15 Topology XV: 6 vertices

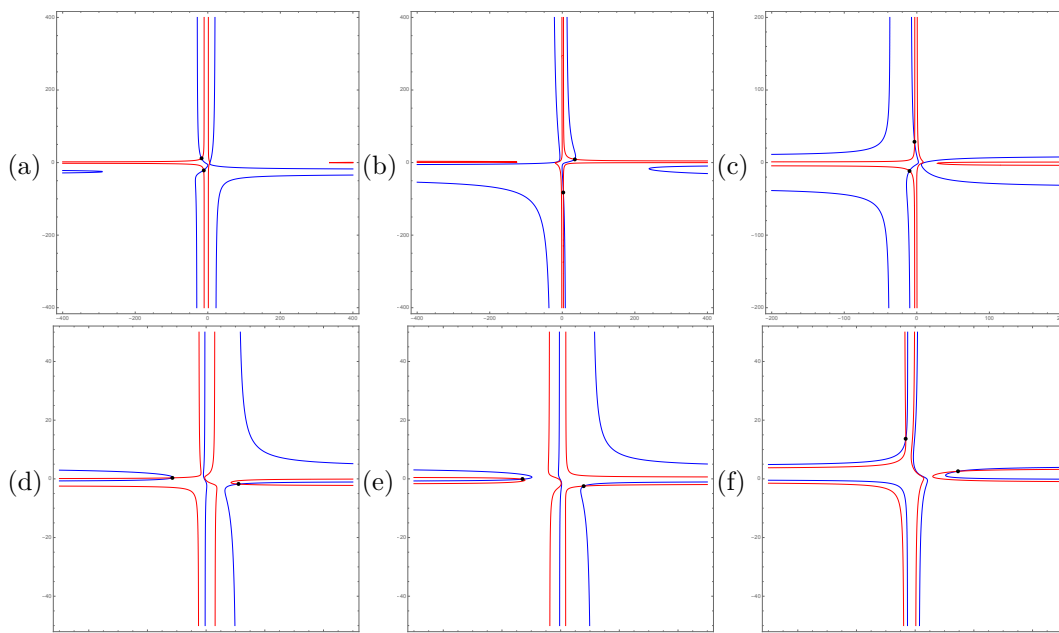
The configuration tuple that induces topology XV is shown in Fig. 69. A set of lines that realizes this tuple, hence this topology, has the following parameters: $(a, b_3, c_3, d_3, e_3, b_4, c_4, d_4, e_4) = (9, 32, -26, 14, 38, 11, -40, 12, -15)$. Fig. 70 shows the six projected bisectors of these four lines, which match the configurations shown in Fig. 69. The $\Gamma(\text{FVD}(L))$ is shown in Fig. 71.



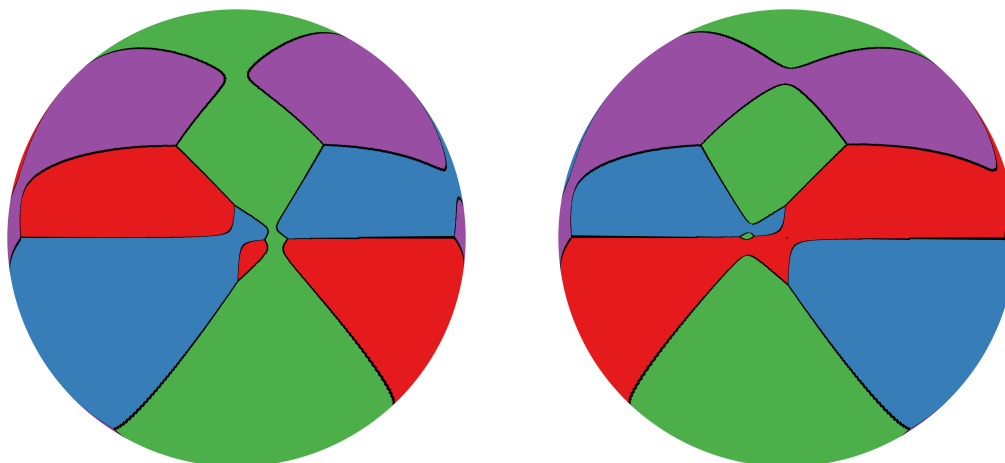
■ **Figure 35** Top and bottom view of $\Gamma(\text{FVD}(L))$ of topology III.



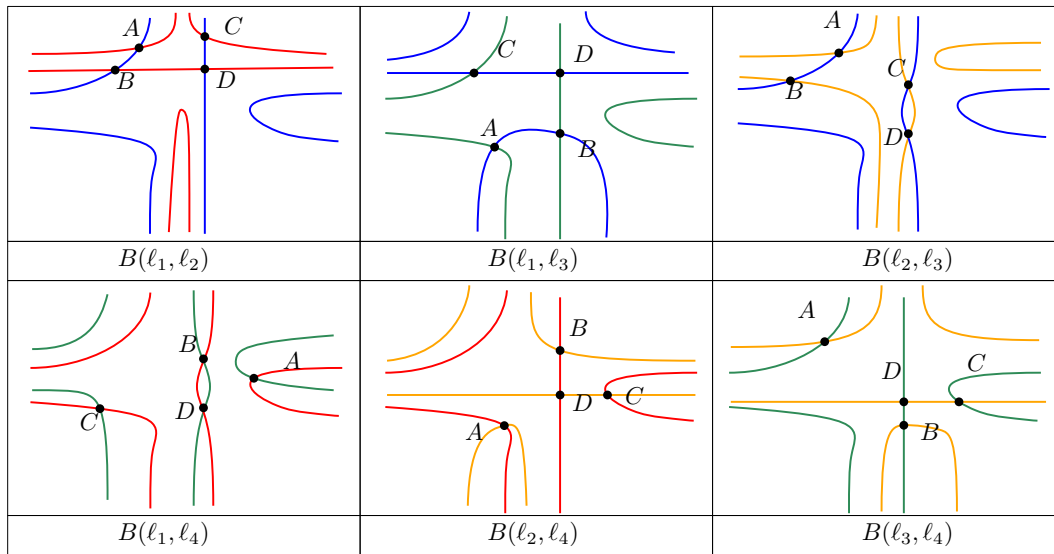
■ **Figure 36** Combination that forms topology IV.



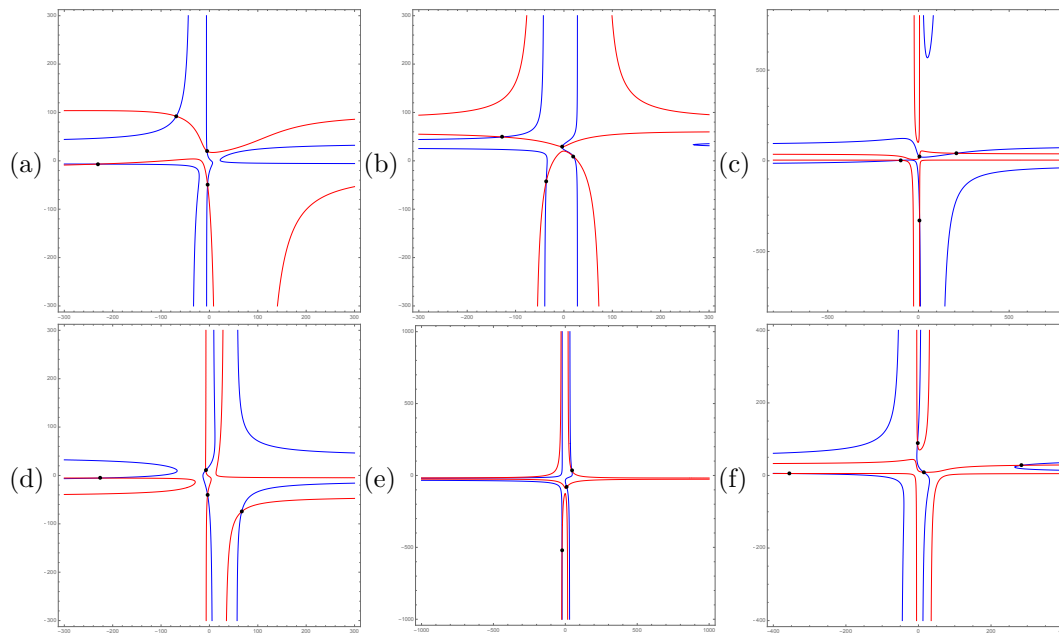
■ **Figure 37** Six projected bisectors when the four lines have the following parameters: $(a, b_3, c_3, d_3, e_3, b_4, c_4, d_4, e_4) = (4, -9, -8, -6, -1, 10, -1, 0, -1)$. They match the configurations shown in Fig. 36 and form topology IV.



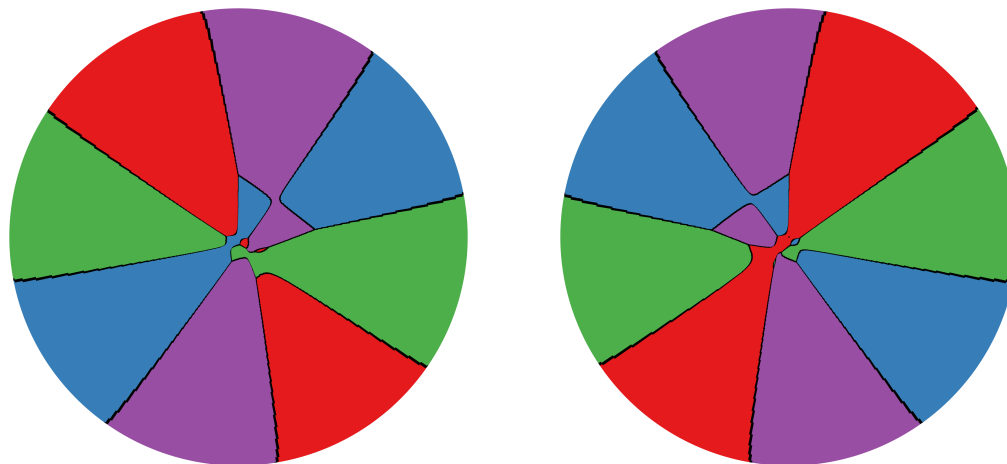
■ **Figure 38** Top and bottom view of $\Gamma(\text{FVD}(L))$ of topology IV.



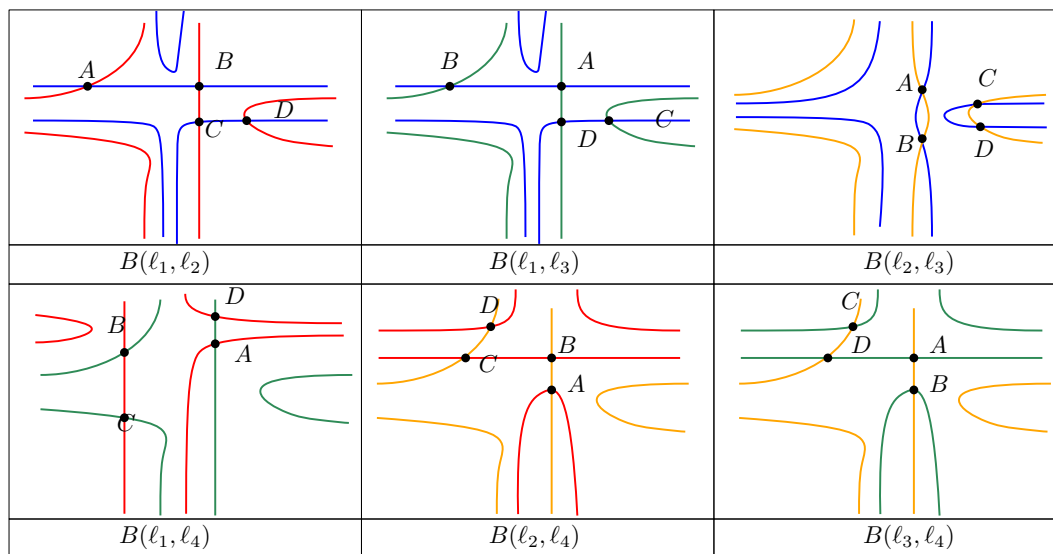
■ **Figure 39** Combination that forms topology V.



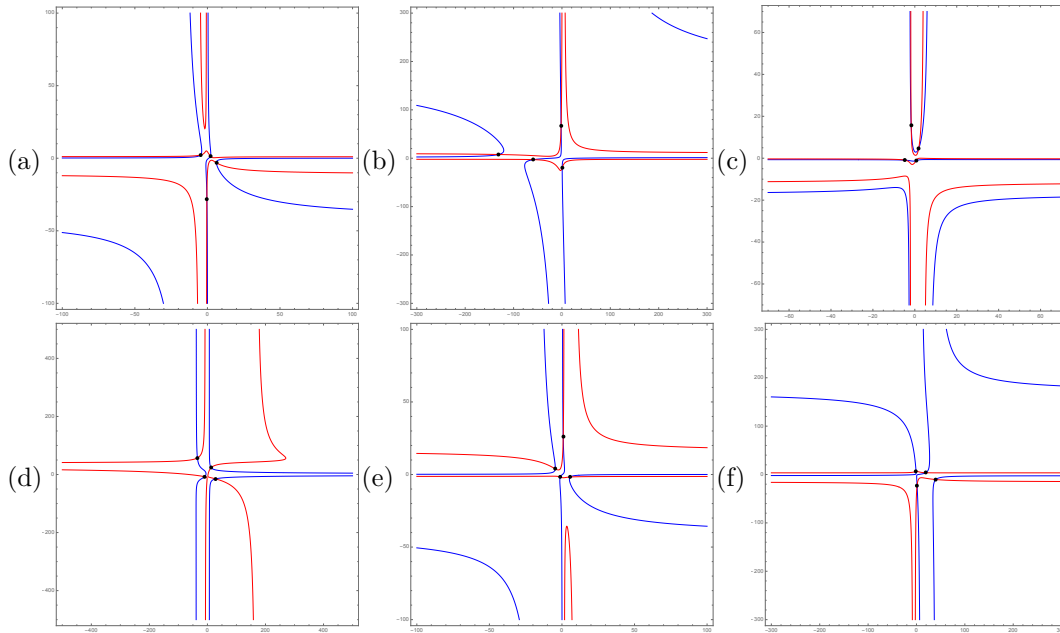
■ **Figure 40** Six projected bisectors when the four lines have the following parameters: $(a, b_3, c_3, d_3, e_3, b_4, c_4, d_4, e_4) = (1, -19, 11, 7, 16, -11, 1, -12, 6)$. They match the configurations shown in Fig. 39 and form topology V.



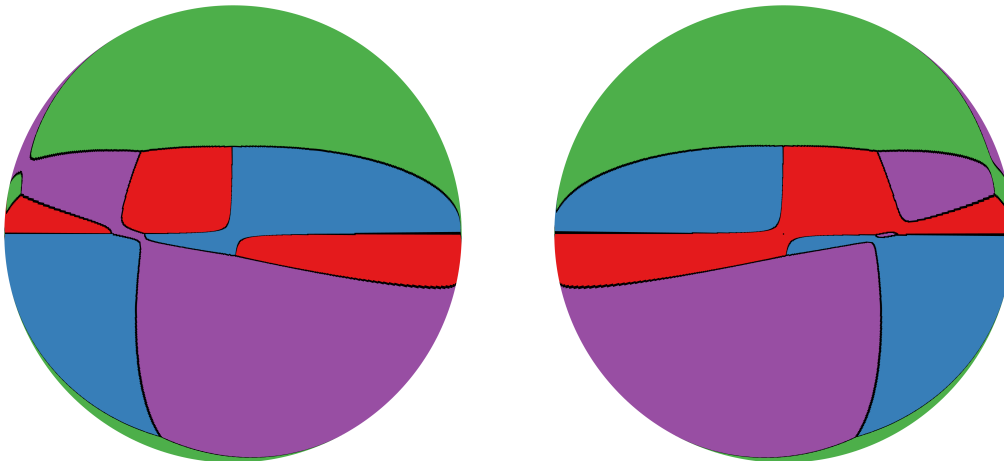
■ **Figure 41** Top and bottom view of $\Gamma(\text{FVD}(L))$ of topology V.



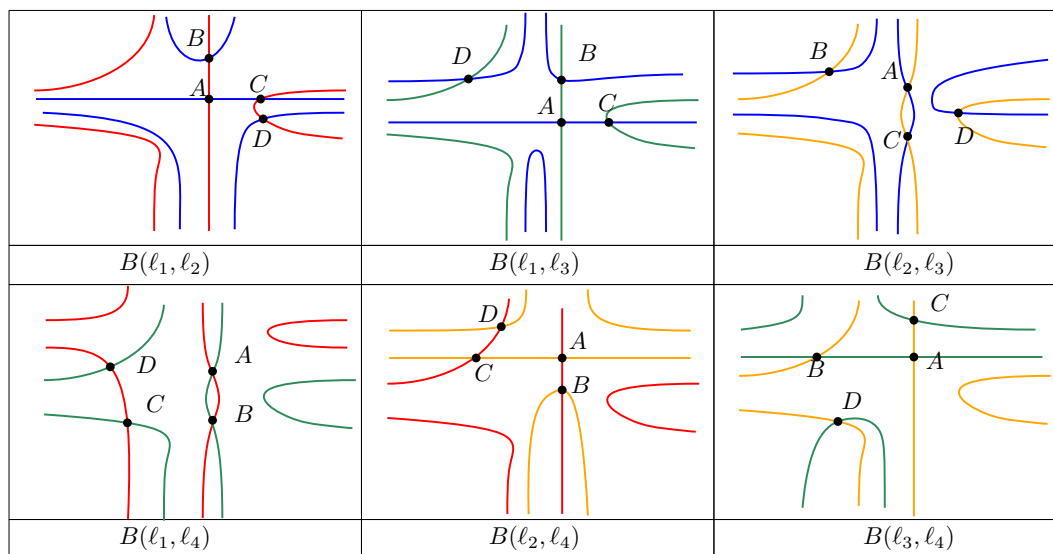
■ **Figure 42** Combination that forms topology VI.



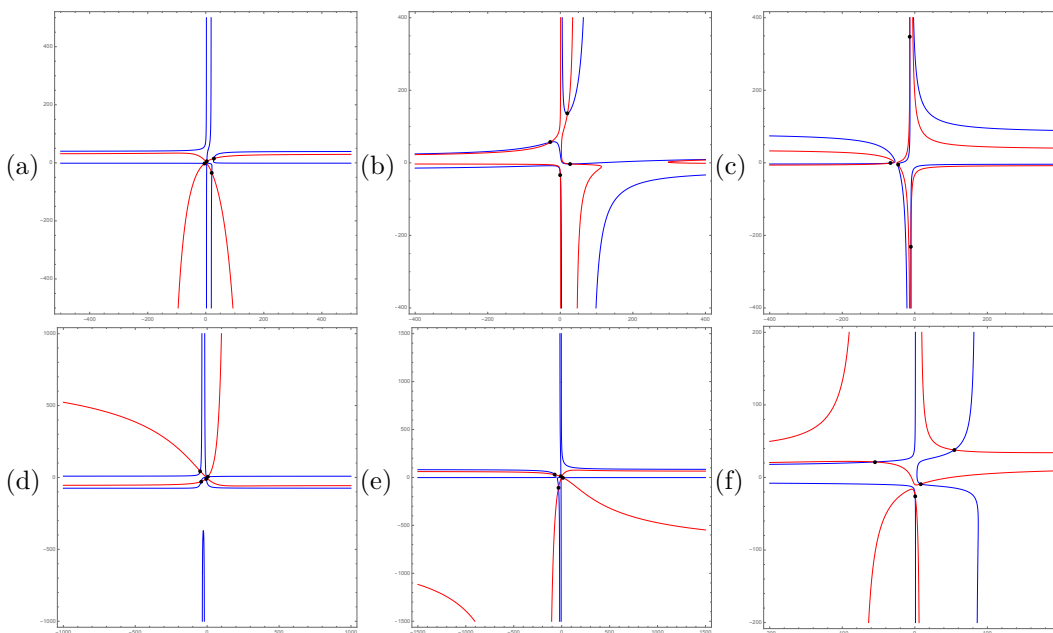
■ **Figure 43** Six projected bisectors when the four lines have the following parameters: $(a, b_3, c_3, d_3, e_3, b_4, c_4, d_4, e_4) = (16, -10, 3, 0, -1, 5, 1, 2, 5)$. They match the configurations shown in Fig. 42 and form topology VI.



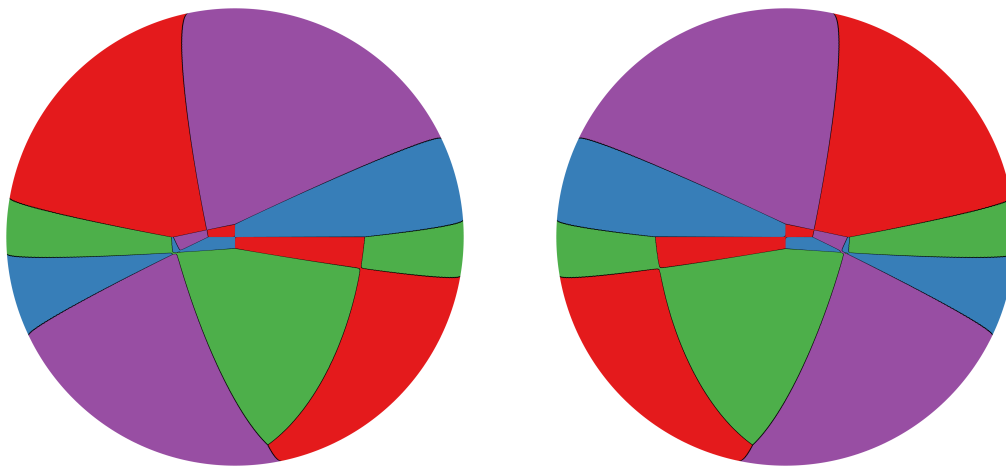
■ **Figure 44** Top and bottom view of $\Gamma(\text{FVD}(L))$ of topology VI.



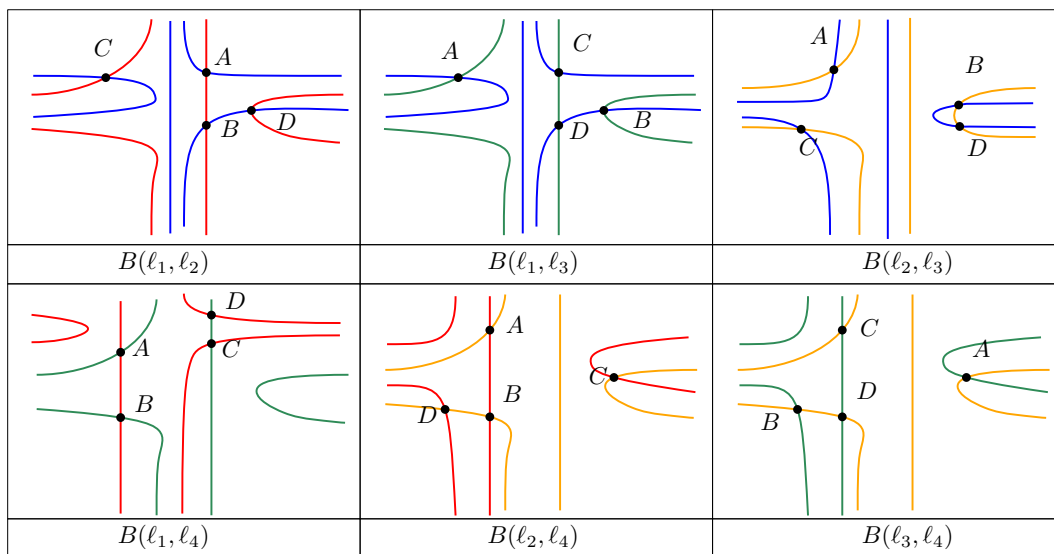
■ **Figure 45** Combination that forms topology VII.



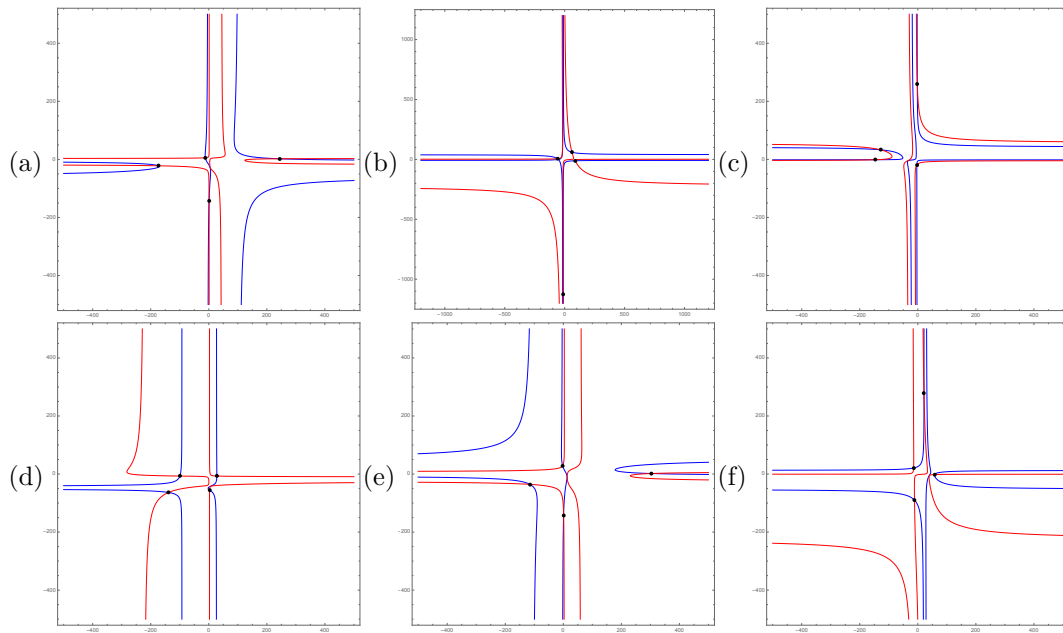
■ **Figure 46** Six projected bisectors when the four lines have the following parameters: $(a, b_3, c_3, d_3, e_3, b_4, c_4, d_4, e_4) = (4, 7, 9, 1, 10, -3, -10, 6, -8)$. They match the configurations shown in Fig. 45 and form topology VII.



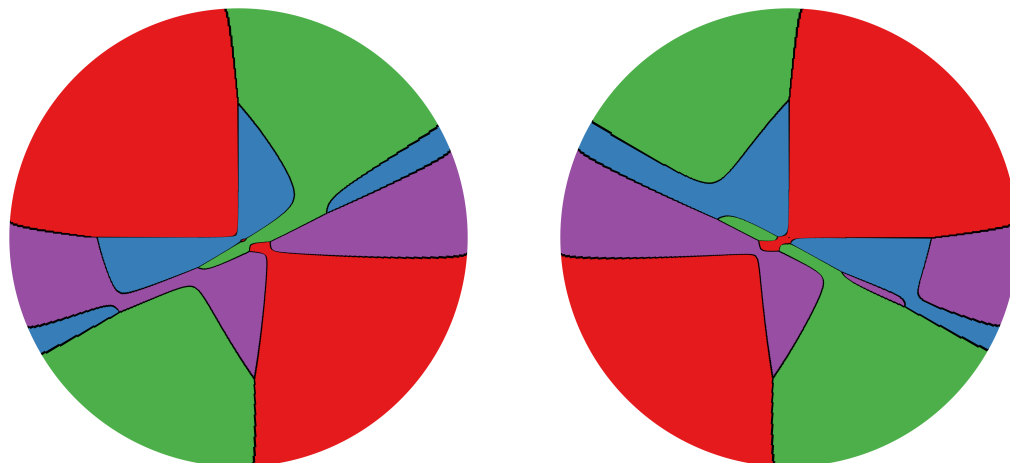
■ **Figure 47** Top and bottom view of $\Gamma(\text{FVD}(L))$ of topology VII.



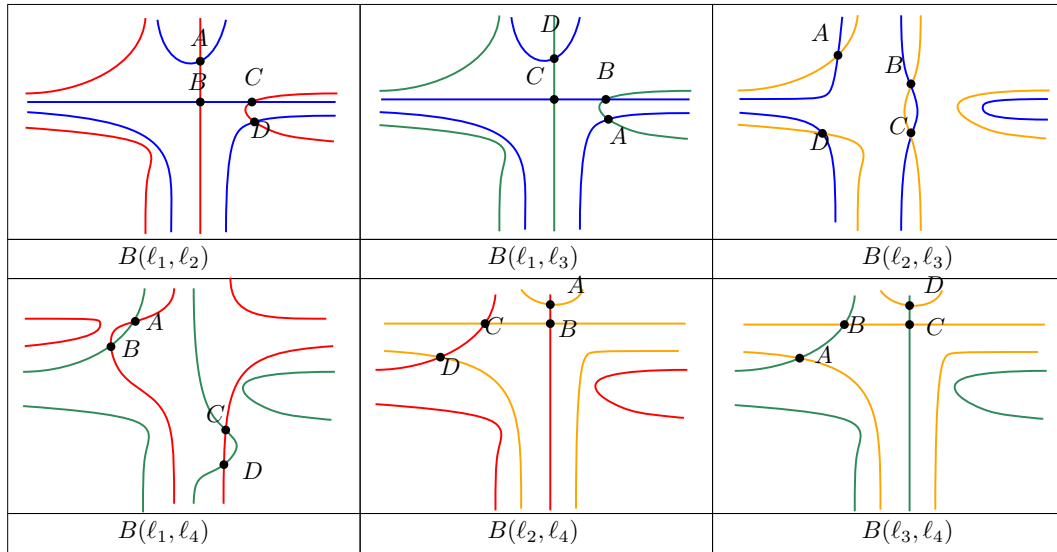
■ **Figure 48** Combination that forms topology VIII.



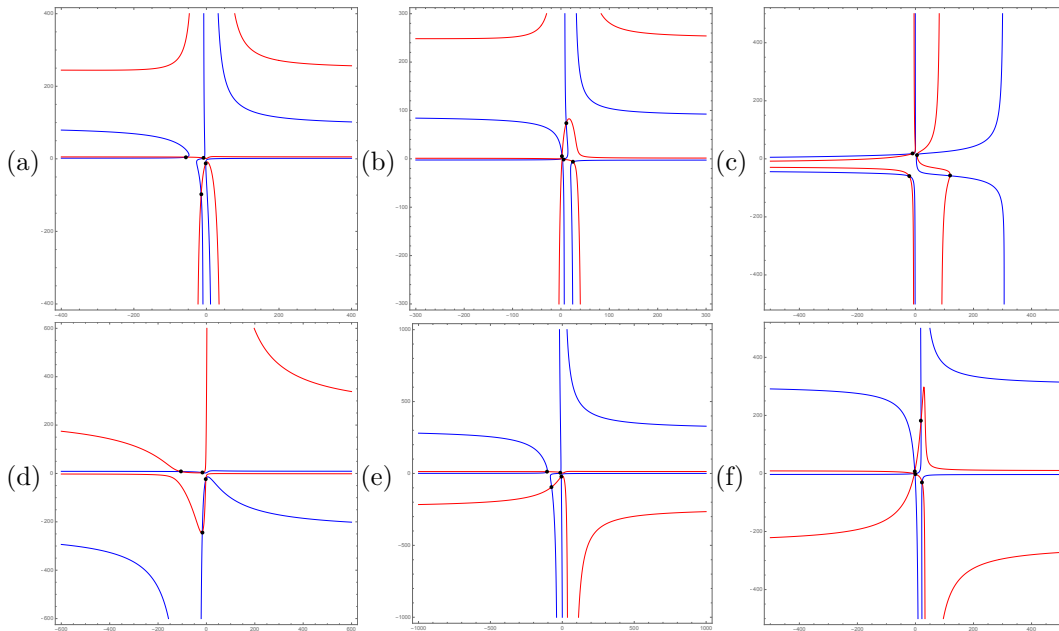
■ **Figure 49** Six projected bisectors when the four lines have the following parameters: $(a, b_3, c_3, d_3, e_3, b_4, c_4, d_4, e_4) = (2, -19, -4, -13, 20, 14, -18, -3, 9)$. They match the configurations shown in Fig. 48 and form topology VIII.



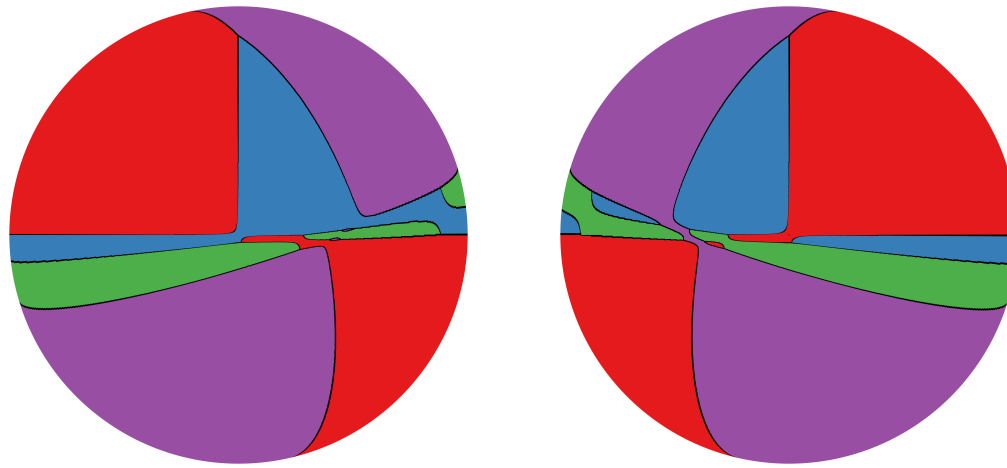
■ **Figure 50** Top and bottom view of $\Gamma(\text{FVD}(L))$ of topology VIII.



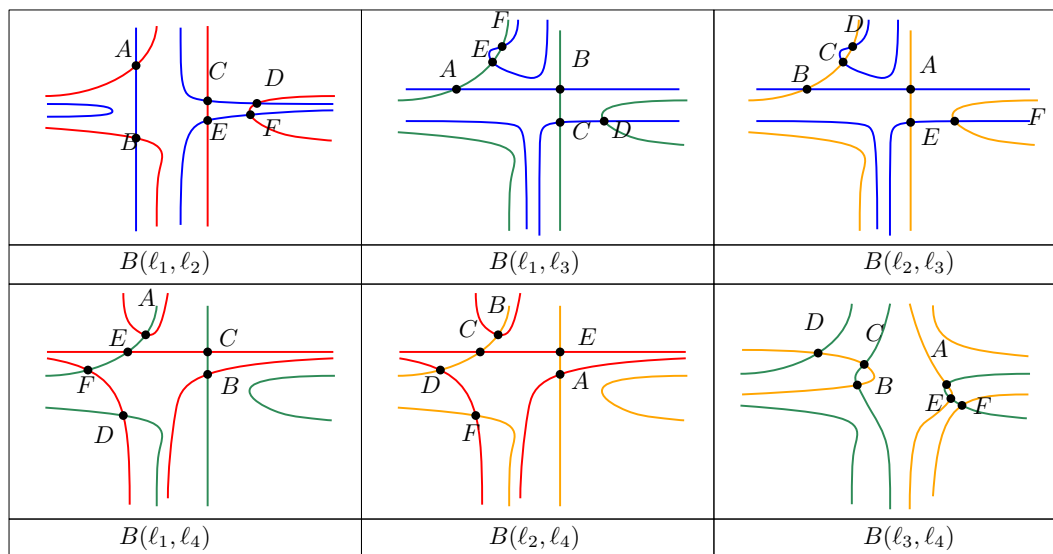
■ **Figure 51** Combination that forms topology IX.



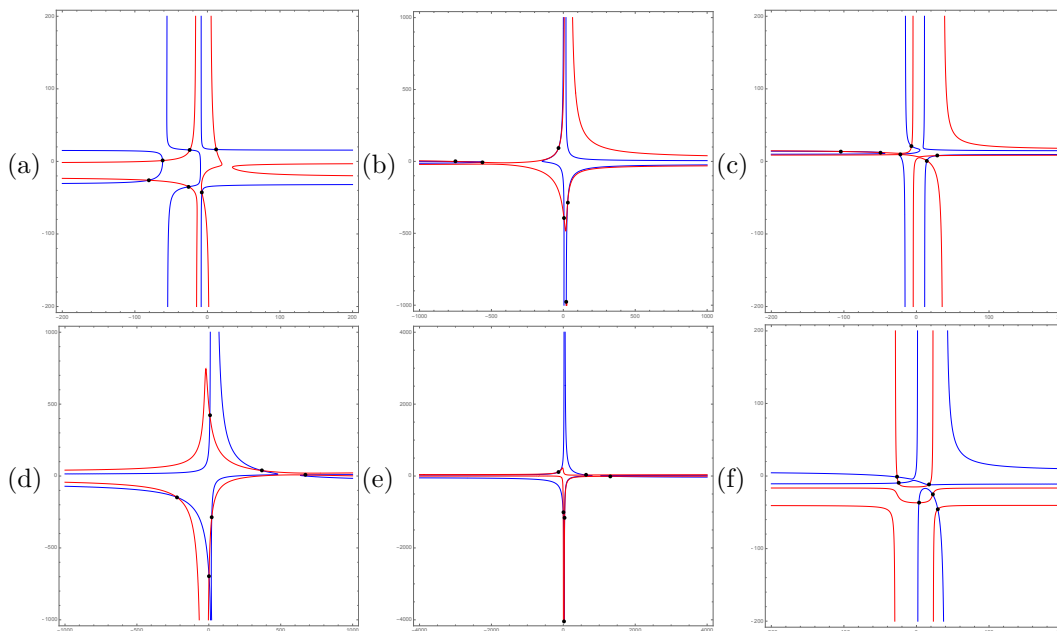
■ **Figure 52** Six projected bisectors when the four lines have the following parameters: $(a, b_3, c_3, d_3, e_3, b_4, c_4, d_4, e_4) = (10, 8, -15, -2, 15, 12, 9, -2, 4)$. They match the configurations shown in Fig. 51 and form topology IX.



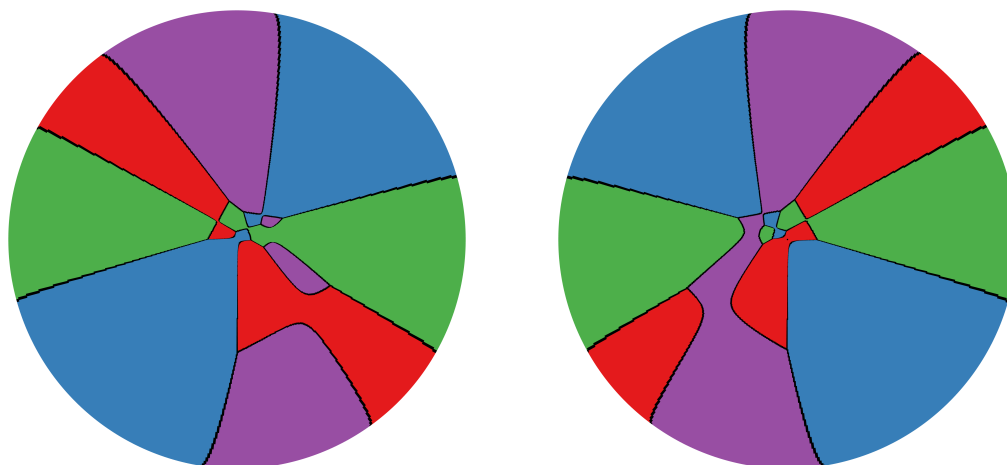
■ **Figure 53** Top and bottom view of $\Gamma(\text{FVD}(L))$ of topology IX.



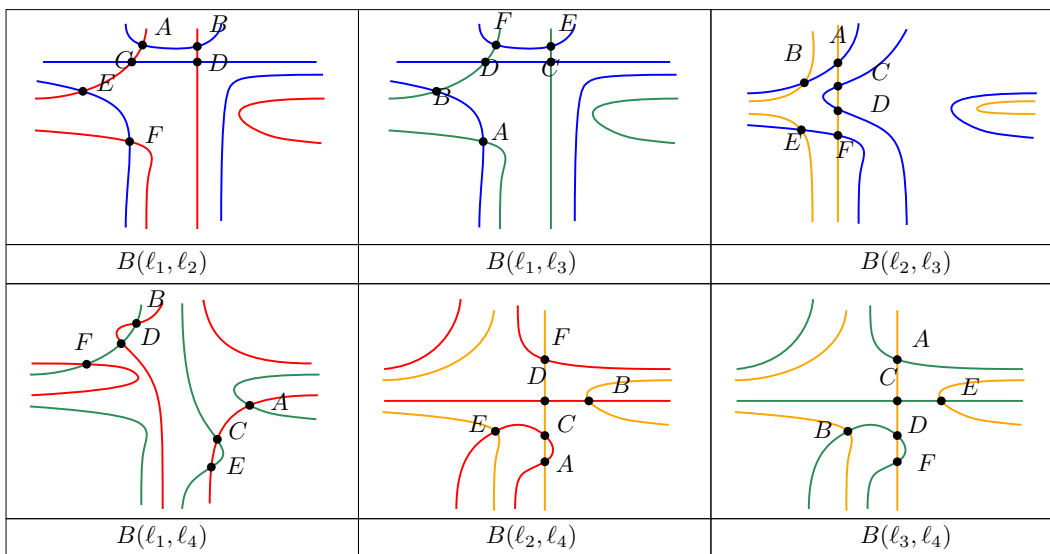
■ **Figure 54** Combination that forms topology X.



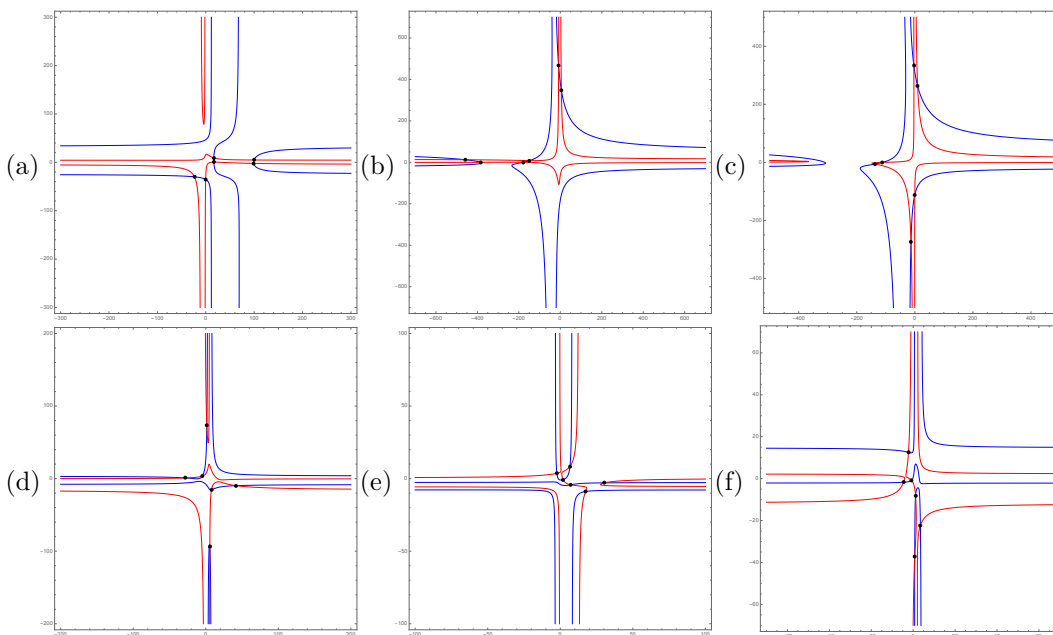
■ **Figure 55** Six projected bisectors when the four lines have the following parameters: $(a, b_3, c_3, d_3, e_3, b_4, c_4, d_4, e_4) = (1, -18, -5, -4, -16, 11, -18, -6, -3)$. They match the configurations shown in Fig. 54 and form topology X.



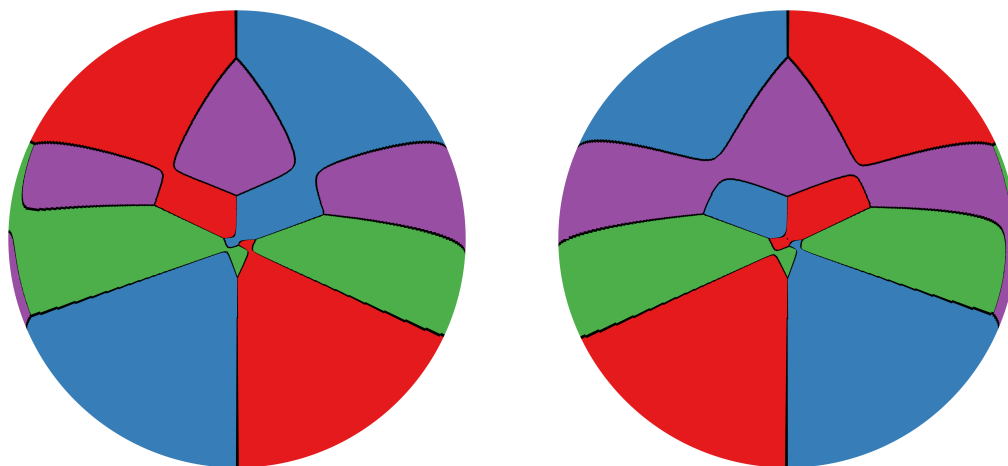
■ **Figure 56** Top and bottom view of $\Gamma(\text{FVD}(L))$ of topology X.



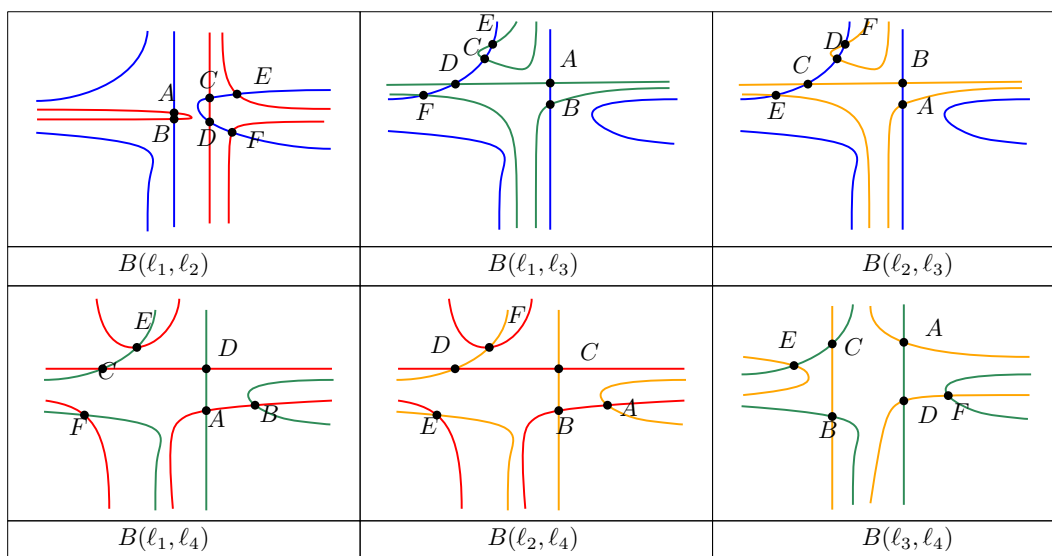
■ **Figure 57** Combination that forms topology XI.



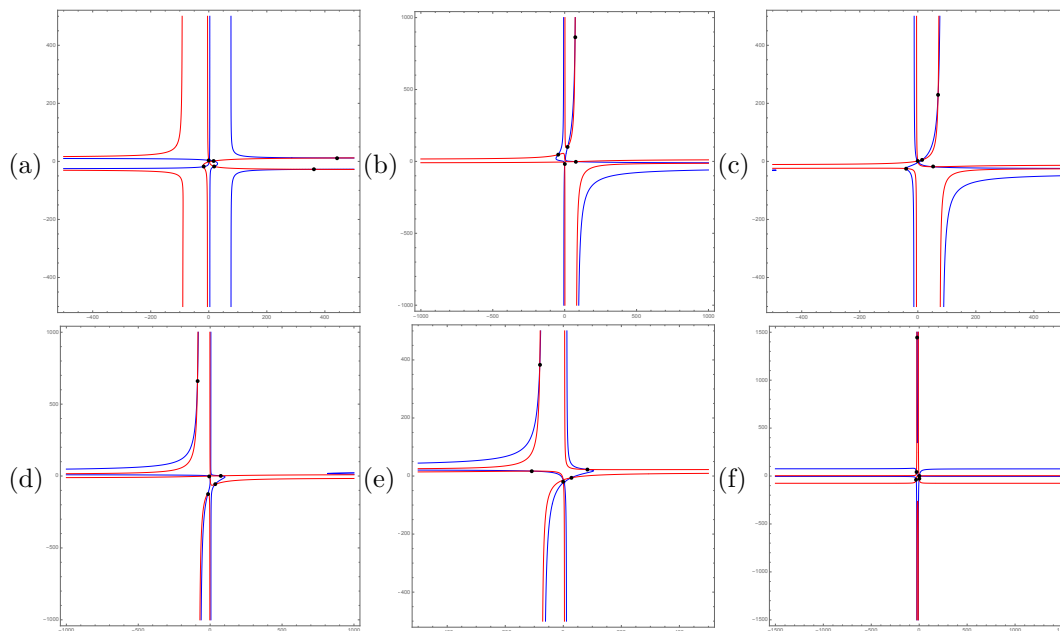
■ **Figure 58** Six projected bisectors when the four lines have the following parameters: $(a, b_3, c_3, d_3, e_3, b_4, c_4, d_4, e_4) = (1, 29, 4, 2, 20, 11, 25, 0, -3)$. They match the configurations shown in Fig. 57 and form topology XI.



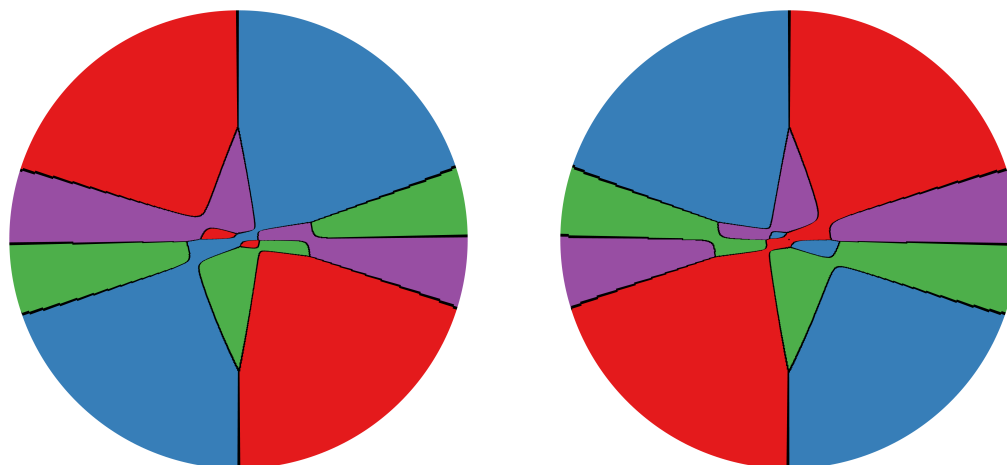
■ **Figure 59** Top and bottom view of $\Gamma(\text{FVD}(L))$ of topology XI.



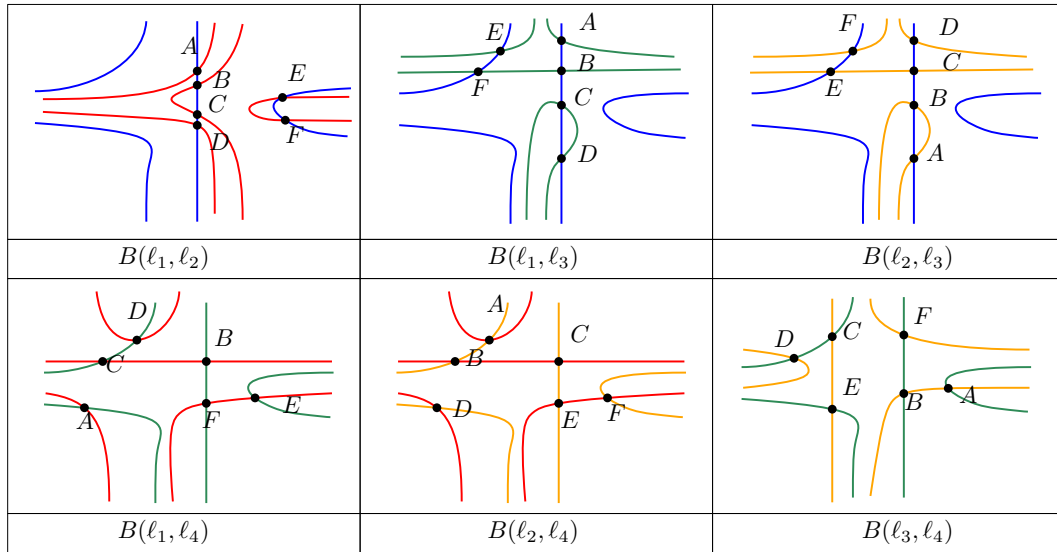
■ **Figure 60** Combination that forms topology XII.



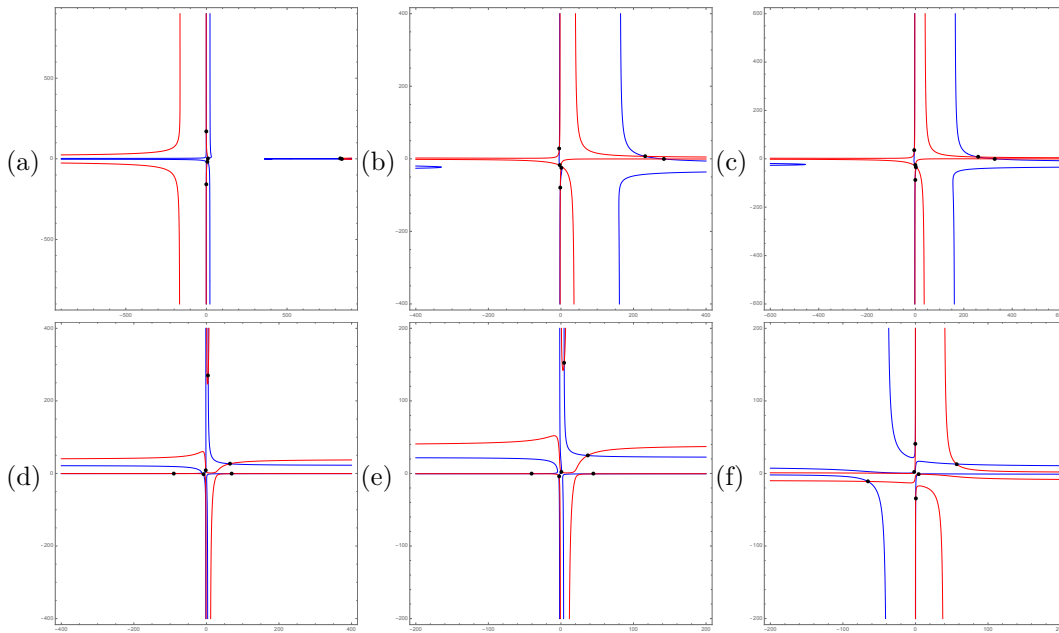
■ **Figure 61** Six projected bisectors when the four lines have the following parameters: $(a, b_3, c_3, d_3, e_3, b_4, c_4, d_4, e_4) = (2, 3, -6, -3, 16, -1, -12, -3, -19)$. They match the configurations shown in Fig. 60 and form topology XII.



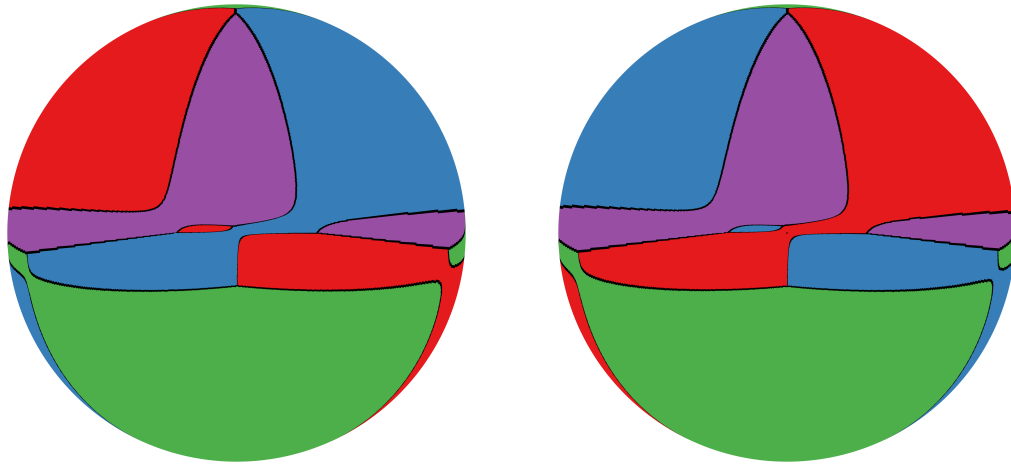
■ **Figure 62** Top and bottom view of $\Gamma(\text{FVD}(L))$ of topology XII.



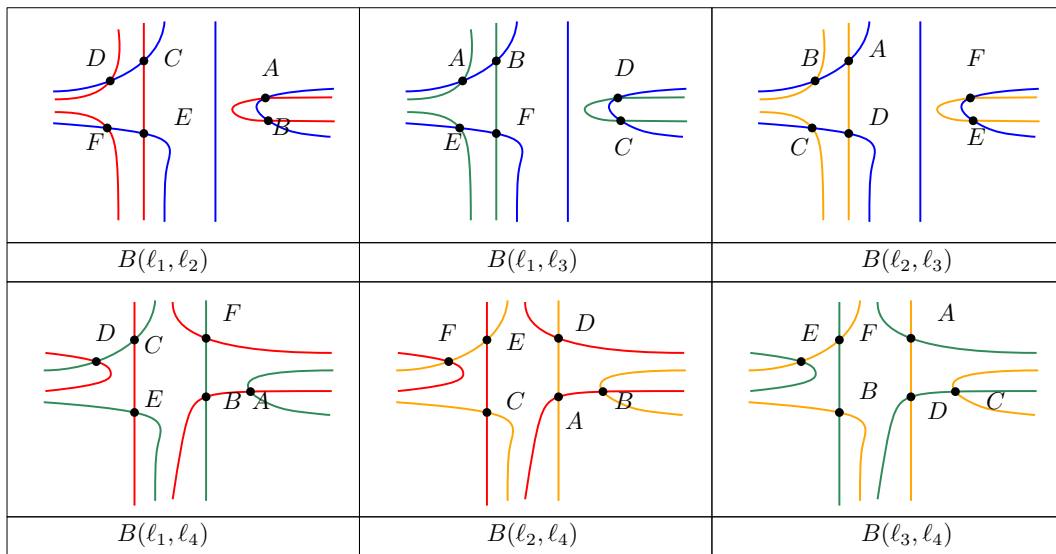
■ **Figure 63** Combination that forms topology XIII.



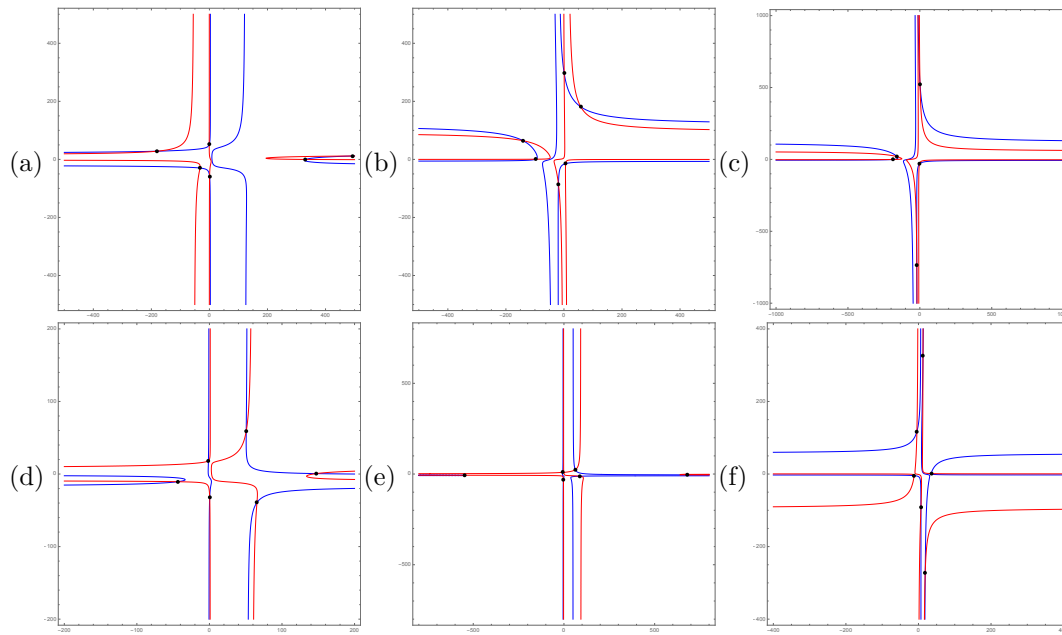
■ **Figure 64** Six projected bisectors when the four lines have the following parameters: $(a, b_3, c_3, d_3, e_3, b_4, c_4, d_4, e_4) = (5, 7, -10, 0, 2, 16, 7, 0, -16)$. They match the configurations shown in Fig. 63 and form topology XIII.



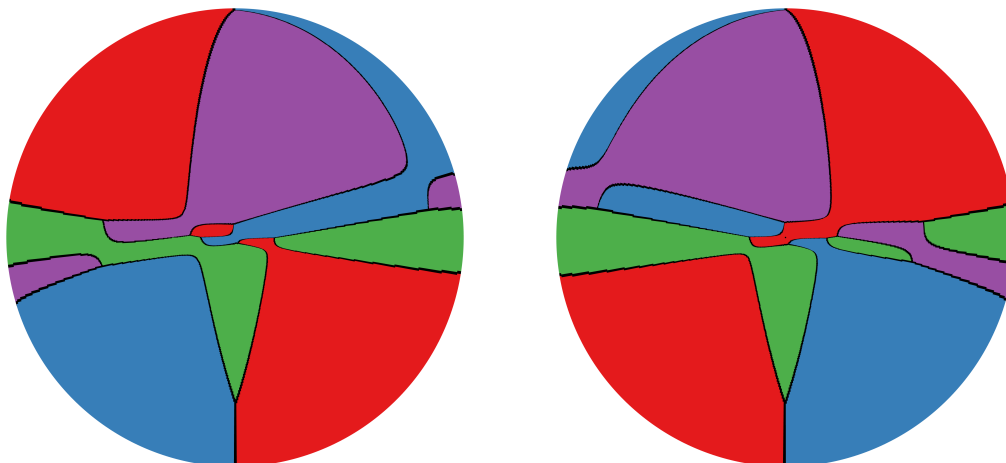
■ **Figure 65** Top and bottom view of $\Gamma(\text{FVD}(L))$ of topology XIII.



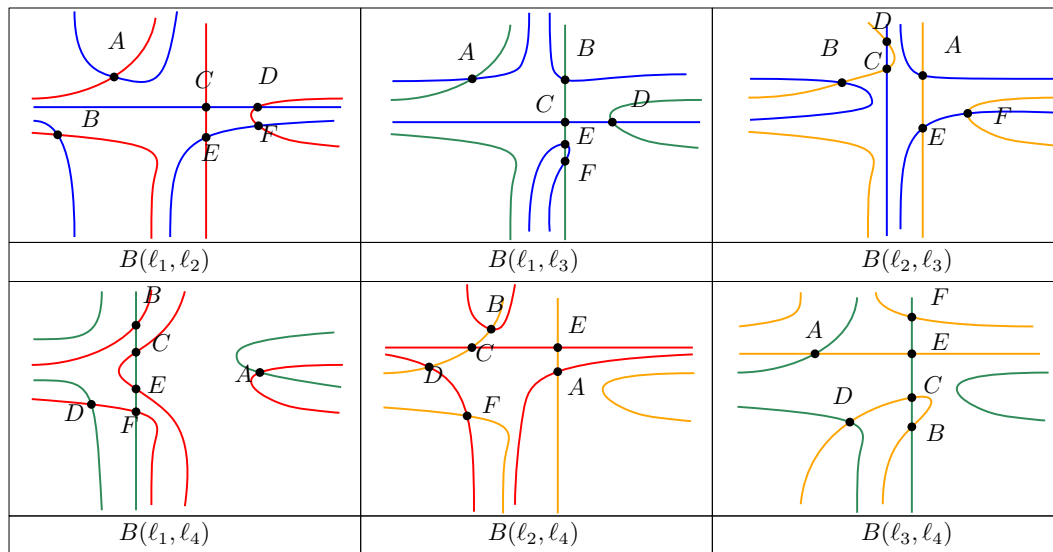
■ **Figure 66** Combination that forms topology XIV.



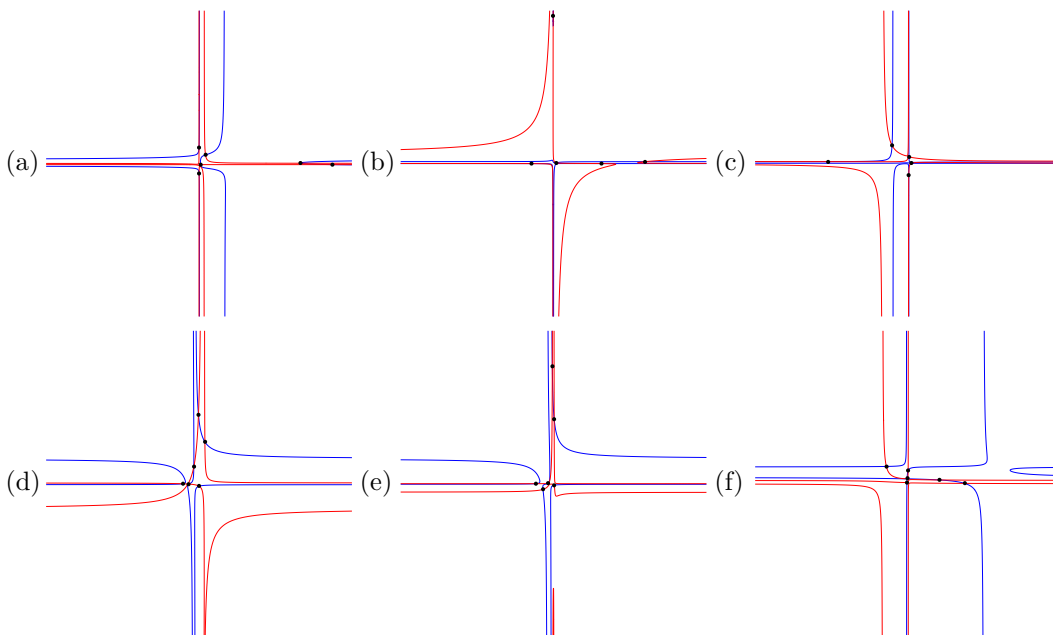
■ **Figure 67** Six projected bisectors when the four lines have the following parameters: $(a, b_3, c_3, d_3, e_3, b_4, c_4, d_4, e_4) = (3, 17, 9, 0, 19, 11, -16, 2, -8)$. They match the configurations shown in Fig. 66 and form topology XIV.



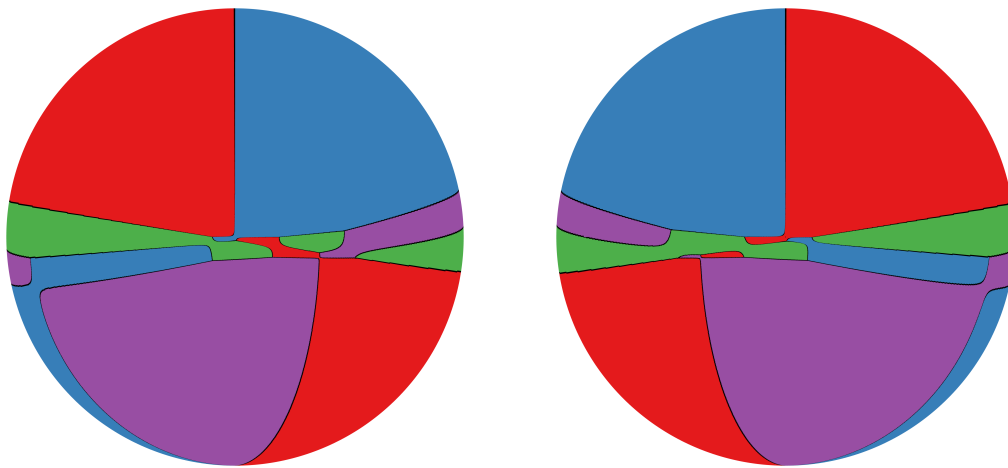
■ **Figure 68** Top and bottom view of $\Gamma(\text{FVD}(L))$ of topology XIV.



■ **Figure 69** Combination that forms topology XV.



■ **Figure 70** Six projected bisectors when the four lines have the following parameters: $(a, b_3, c_3, d_3, e_3, b_4, c_4, d_4, e_4) = (9, 32, -26, 14, 38, 11, -40, 12, -15)$. They match the configurations shown in Fig. 69 and form topology XV.



■ **Figure 71** Top and bottom view of $\Gamma(\text{FVD}(L))$ of topology XV.

